Geophysical Journal International

Geophys. J. Int. (2010) **182,** 1411–1430 doi: 10.1111/j.1365-246X.2010.04685.x

Kinematic rupture process of the 2007 Tocopilla earthquake and its main aftershocks from teleseismic and strong-motion data

S. Peyrat,[1] R. Madariaga,[2] E. Buforn,[3] J. Campos,[4] G. Asch[5] and J. P. Vilotte[1]

[1] *Institut de Physique du Globe,* 4 *Place Jussieu,* 75251 *Paris Cedex* 05, *France. E-mail: peyrat@ipgp.jussieu.fr*
[2] *Laboratoire de Géologie CNRS-Ecole Normale Supérieure,* 75231 *Paris Cedex* 05, *France*
[3] *Departamento de Geofísica y Meteorología, Facultad de Ciencias Físicas, Univ. Complutense,* 28040 *Madrid, Spain*
[4] *Departamento de Geofísica, Universidad de Chile, Casilla* 2777, *Santiago, Chile*
[5] *GFZ Potsdam Telegrafenberg PB* 2.4, D-14473 *Potsdam, Germany*

Accepted 2010 May 31. Received 2010 May 23; in original form 2009 February 23

SUMMARY

We study a large $M_w = 7.6$ earthquake that occurred on 2007 November 14 in the Northern Chile seismic gap near the city of Tocopilla. Using a variety of seismic data we show that this earthquake ruptured only the lower part of the interplate seismic zone and generated a series of plate interface aftershocks. Two large aftershocks on 2007 November 15 ruptured the interplate zone oceanwards of the Mejillones Peninsula, a major geographical feature in the Antofagasta region. On 2007 December 16, a large $M_w = 6.8$ aftershock, that occurred near the southern bottom of the fault plane of the main event, is shown to be a slab-push earthquake located inside the subducted Nazca Plate and triggered by along slab compression. Aftershocks of this event demonstrate that it occurred on an almost vertical fault. The Tocopilla earthquake took place just after the installation of a new seismological network by Chilean, German and French researchers. The accelerometric data combined with far field seismic data provide a quite complete and consistent view of the rupture process. The earthquake broke a long (130 km) and narrow (about 30–50 km) zone of the plate interface just above the transition zone. Using a non-linear kinematic inversion method, we determined that rupture occurred on two well-defined patches of roughly elliptical shape. We discuss the consequences of this event for models of gap filling earthquakes in Chile proposed in the 1970s.

Key words: Earthquake ground motions; Earthquake source observations; Seismicity and tectonics; Computational seismology; Subduction zone processes; South America.

GJI Seismology

1 INTRODUCTION

A large $M_w = 7.6$ earthquake occurred at 15:40:50 (UTC) on 2007 November 14 in Northern Chile between 22°S and 23°S in a region that has long been identified as a potential seismic gap (Kelleher 1972; Kelleher *et al.* 1973). The earthquake occurred in the area just North of the rupture zone of the $M_w = 8$ Antofagasta earthquake of 1995 July 30 (Ruegg *et al.* 1996; Delouis *et al.* 1997; Chlieh *et al.* 2004; Pritchard & Simons 2006). The Tocopilla earthquake is very interesting because it is the first large Chilean event to be recorded by a network of digital accelerometers and broad-band stations. The earthquake occurred in a largely deserted area so that damage was concentrated in a couple of locations, mainly the city of Tocopilla and the mining town of Maria Elena (Astroza *et al.* 2008).

In the 1970s and 1980s, several gaps were identified along the Chilean subduction zone based mainly on data obtained by Chilean historians and interpreted by Montessus de Ballore (1911–1916) and Lomnitz (1971). A long-standing discussion ensued as to whether those gaps are semi-permanent features of the subduction zone limited by barriers or simply reflect the largest events in recent history (see, e.g. Comte *et al.* 1986; Madariaga 1998). Because Northern Chile was very lightly inhabited until the beginning of last century, information about historical earthquakes is very scant. Geodetic and seismological data for Northern Chile seems to indicate that the region of the Tocopilla earthquake was fully locked with little or no slip occurring on the seismogenic zone above the transition zone from continuous to stick slip. The 2007 November 14 event is the largest thrust event that has taken place for almost 150 years inside the Northern Chile gap. A detailed study of this event provides crucial insights regarding the way a large seismic gap will eventually rupture as well as the way to improve the monitoring of the gap as it comes up back to activity. The lessons from this event may be useful to understand the awakening of seismicity in other long-standing quiescence zones.

The Tocopilla earthquake offers a unique opportunity to understand many issues connected with the rupture of the locked interplate interface in Chile. The event was very well recorded by the global seismic networks, and it occurred in an area where seismological and geodetic instruments were recently deployed. A new permanent continuously recording broadband and strong-motion network was recently installed as a join effort by the Helmhotz-Zentrum Potsdam, Deutsches GeoForschungsZentrum (GFZ) of Germany,

by Institut de Physique du Globe de Paris (IPGP) of France and the Geophysics Department of University of Chile in Santiago (DGF), through the International Plate Boundary Observatory Chile (IPOC) project (see Schurr *et al.* 2009). The Tocopilla earthquake and a few of its aftershocks were also very well recorded by a triggered strong-motion network operated by the University of Chile in collaboration with German and Swiss institutions (see Boroschek *et al.* 2008). A first study of the earthquake was recently published by Delouis *et al.* (2009) who modelled the main event using far field data and the accelerograms from the triggered network.

In this paper, we investigate the detail rupture process of the Tocopilla earthquake ($M_w = 7.6$) of the 2007 November 14 and of its two main aftershocks using all available seismic data (teleseismic and strong-motion data). We compare the results obtained using the far-field and near-field seismic data with the aftershock distribution determined by Lancieri *et al.* (2009) and Ruiz *et al.* (2009). On the basis of these observations, we present a two step model of the source process of the mainshock and its three larger aftershocks. In a parallel study, Béjar-Pizarro *et al.* (2010) studied the geodetic field produced by the earthquake using both GPS and interferometric data. We finally compute coulomb stress change to examine the hypothesis that aftershocks were triggered by stress changes from the mainshock.

2 TECTONIC SETTING AND SEISMICITY OF NORTHERN CHILE

Chile exhibits a strong seismicity with frequent large thrust earthquakes that originate on the plate interface between the subducted Nazca Plate and the South American Plate. These events are the consequence of the subduction of the Nazca Plate beneath South America at a high convergence rate (6.6 cm yr^{-1}) (Angermann *et al.* 1999). Occasionally, large intermediate depth events occur inside the Nazca Plate below the coupled interface. Shallow crustal events are rare and do not reach the large magnitudes of the largest events due to subduction. In Northern Chile, the largest of these events, $M_w = 6.3$, took place in on 2001 July 21 (see Legrand *et al.* 2007).

Although there is little paleoseismological information, the seismicity of Chile since 1600 is relatively well known, thanks to historical documents gathered by historians and seismologists (Montessus de Ballore 1911–1916; Lomnitz 1971, 2004; Comte & Pardo 1991). From these works it appears that along the Chilean coast the plate interface is at very different stages of the seismic cycles. The differences are clear: Southern Chile, South of 36°S experienced the May 1960 mega earthquake; Central Chile, on the other hand, is currently very active with magnitude 8 events occurring at regular intervals of about 80 years (Comte *et al.* 1986; Beck *et al.* 1998). The situation in Northern Chile, where the Tocopilla event occurred, is quite interesting: as shown in Fig. 1 two mega earthquakes occurred in Northern Chile and Southern Peru in the second half of the 19th century (Kausel 1986; Comte & Pardo 1991). In the Antofagasta region, where the 2007 Tocopilla earthquake occurred, the last mega-thrust event took place in May 1877 with an epicentral area near Iquique ($M_w = 8.9$; Kausel 1986). The fault area of the 1877 event shown in Fig. 1 is relatively well known, thanks to studies of the effects of the earthquake and the careful evaluation of the tsunami it generated (Kausel 1986; Comte & Pardo 1991). The source area of the other large $M_w > 8.7$ earthquake that occurred in August 1868 in Southern Peru and, partly, in Northern Chile has recently seen a revival of activity with the large 2001 Arequipa earthquake ($M_w = 8.4$) that partly filled the rupture zone of the 1868 earthquake (Giovanni

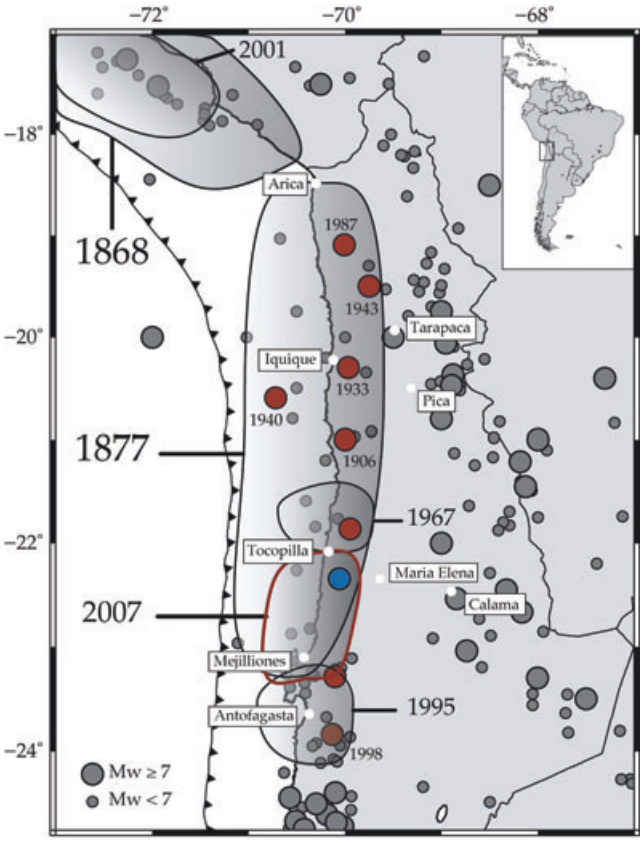

Figure 1. Tectonic setting: location and rupture areas of large earthquakes of the 19th and 20th in Northern Chile shown as estimated rupture zones (from Lomnitz 2004; Comte & Pardo 1991). Seismicity of magnitude greater than 5.5 (grey circles) from the Centennial Catalog (Engdahl & Villaseñor 2002). Red circles are events from Table 1. Blue circle is the 2007 November 14 Tocopilla mainshock. White dots are the main places named in the text.

et al. 2002; Robinson *et al.* 2006). In a recent paleoseismological study of the Mejillones Peninsula, Vargas *et al.* (2005) found at least two mega-thrust events in the period 1409–1449 and 1754–1789, but they found no clear trace of the 1877 event in the Mejillones Peninsula. We interpret this observation as a confirmation that the 1877 event did not propagate as far South as Mejillones.

The regions of Antofagasta and Tarapaca, had been very quiet in the 20th century until a $M_w = 8$ earthquake occurred on 1995 July 30 in Antofagasta (Table 1). This earthquake was very well studied from seismological and geodetic points of view (see, e.g. Delouis

Table 1. Seismicity of the Northern Chile Gap. Event locations of magnitude greater than 7 were selected from the Centennial Catalog of Engdahl & Villaseñor (2002) (events deeper than 80 km are not included).

Date	Time	Lon. (°)	Lat. (°)	Depth (km)	M_w
1905/04/26	21:43:0.00	−70.00	−21.00	60.0	7.0
1906/08/30	2:38:0.00	−70.00	−21.00	0.0	7.1
1933/02/23	8:9:20.78	−69.96	−20.30	35.0	7.2
1940/10/04	7:54:50.11	−70.72	−20.59	23.5	7.1
1943/12/01	10:34:46.00	−69.75	−19.50	80.0	7.1
1967/12/21	2:25:24.40	−69.95	−21.86	42.5	7.4
1987/08/08	15:48:58.05	−70.01	−19.09	71.2	7.2
1995/07/30	5:11:25.16	−70.10	−23.28	46.0	8.0
1998/01/30	12:16:10.46	−70.13	−23.84	42.0	7.1
2001/06/23	20:33:14.98	−73.55	−16.30	29.8	8.4

et al. 1997; Chlieh *et al.* 2004). It ruptured the plate interface for more than 180 km southwards from the Mejillones Peninsula and was followed in 1998 by a large deep aftershock that created additional slip at the plate interface (Ruegg *et al.* 1996; Chlieh *et al.* 2004; Pritchard & Simons 2006; Pritchard *et al.* 2006). As shown in Fig. 1, according to historical studies reported by Comte & Pardo (1991), the area affected by the Antofagasta earthquake of 1995 may have not slipped in 1877.

The Tocopilla earthquake is also interesting from the point of view of the study of seismic gaps in subduction zones. In the early 1970s, several authors (e.g. Kelleher 1972; Kelleher *et al.* 1973; McCann *et al.* 1979) identified the sites of recent large earthquakes as possible seismic gaps, defined as regions that had not experienced a large earthquake for the last 30 years. In hindsight, this period of time is too short to characterize the seismicity produced by subduction of the Nazca Plate under South America (see Cisternas *et al.* 2005, for a recent discussion). The seismic gap concept was originally proposed as a long-term forecast of major earthquakes (see, e.g. McNally 1983; Nishenko 1985). The Northern Chile subduction zone North of 23°N was identified by these authors as important gap, with the potential of harbouring mega earthquakes. From information of past earthquakes and assuming a constant tectonic loading, it was proposed that the next mega-thrust event in Northern Chile would break the northern Chile gap from roughly 23° to 18° North. Some authors proposed that it would break at least the northern half of the fault area of the 1877 earthquake (Casarotti & Piersanti 2003). As shown in Fig. 1, it is clear that the Tocopilla earthquake ruptured less than 20 per cent, of the Northern Chile gap.

The seismicity in the subduction zone of Northern Chile was weak during most of the 20th century with only a few events of $7 < M_w < 7.5$ near the coast. Because of poor earthquake locations during the earlier part of the 20th century, the only reasonably complete data set available is the centennial catalogue of Engdahl & Villaseñor (2002). Fig. 1 shows all the events of magnitude 5.5 or greater in the centennial catalogue and in Table 1 we list the events shallower than 80 km and magnitude greater than 7. Only 12 events appear in the table, these earthquakes are evenly distributed along the length of the seismic gap (Fig. 1). Comte & Pardo (1991) list in their table II and Fig. 3 an event on 1928 November 20 of $M_w = 7.1$ at 22.5°S, 70.5°W that presumably occurred very close to the epicentre of the November 14 earthquake. This event is not listed in the centennial catalogue so that we decided not to include it in the map of Fig. 1.

An interesting event displayed in Fig. 1 is the 1967 Tocopilla earthquake ($M_w = 7.4$), which occurred at a depth of 46–48 km (Stauder 1973; Malgrange & Madariaga 1983; Tichelaar & Ruff 1991). This event, the largest in the Northern Chile gap since 1877, was located by Malgrange & Madariaga (1983) just north of the 2007 event. It had a shallow thrust mechanism but was followed by several aftershocks with different fault plane solutions and depths from the main event indicating a complex rupture process. As shown in Fig. 1, the rupture area of the 2007 Tocopilla earthquake is quite convincingly bounded by the previous earthquakes of 1967 and 1995.

In contrast to the very low activity of the locked subduction interface in Northern Chile, significant seismic activity occurred at intermediate depth. East of the Tocopilla region, a large $M_w = 8$ intermediate depth earthquake occurred in 1950 (Kausel & Campos 1992) and a large $M_w = 7.7$ intermediate depth earthquake (roughly 100 km) occurred on 2005 June 13 further North near 20°S (Peyrat *et al.* 2006; Delouis & Legrand 2007; Peyrat & Favreau 2010).

3 THE 2007 NOVEMBER 14 $M_w = 7.6$ TOCOPILLA EARTHQUAKE

The $M_w = 7.6$ Tocopilla earthquake occurred on 2007 November 14 at 15:40:50 (UTC) in the southern part of the Northern Chile gap. The earthquake occurred in a region where the Nazca Plate subducts beneath the South American Plate at a rate of 6.6 cm yr^{-1} (Angermann *et al.* 1999). This earthquake is the largest thrust earthquake in the region since the 1995 Antofagasta earthquake. Several thousand of homes were destroyed or damaged and more than 15 000 people were displaced in the Tocopilla and Maria Elena areas. The maximum accelerations were 0.4 g in Tocopilla and Mejillones. The estimated intensities of the Tocopilla earthquake are similar to those of the 1967 earthquake (Astroza *et al.* 2008). Several landslides and pavement cracking were observed in the region. The earthquake also produced a small regional tsunami with wave heights of 25.5 cm at Antofagasta, 19.3 cm at Iquique and 19.5 cm at Arica (Hébert *et al.* 2008). It was followed by several aftershocks, two of them with magnitude larger than 6 occurred on 2007 November 15. Most of the aftershocks have the same thrust mechanism as the mainshock, but on 2007 December 16 at 09:09:17 (UTC) a slab-push aftershock occurred near the southern end of the rupture zone, close to the Mejillones peninsula. This earthquake had a typical slab-push mechanism with *P* -wave polarities that are reversed with respect to those of the main shock. Slab-push events occur quite frequently in Chile, Peru and Mexico (Lemoine *et al.* 2002; Gardi *et al.* 2006).

3.1 Available data

The Tocopilla earthquake and its aftershocks were well recorded on seismological global networks as well as by several recently installed digital accelerometric networks.

IPOC, a permanent seismological network of 12 stations (Fig. 2) was installed in Northern Chile starting in 2006. The purpose of this network was to combine broadband, accelerometer, GPS and tiltmeters with continuous recording and satellite transmission, to detect changes in seismicity and to improve the current instrumentation in Northern Chile. The network became operational in 2006; most of the seismological stations are composed of STS-2 broadband seismometers, GMG-5 accelerometers for the French stations and Episensor FBA ES-T for the German stations, continuously recording at 100 Hz with 24 bit Q330 digitizers and SeiscomPC (http://geofon.gfz-potsdam.de/geofon/seiscomp). We also used the strong-motion data recorded by a permanent digital strong motion network operated jointly by the University of Chile, Swiss and German institutions (Boroschek *et al.* 2008; Delouis *et al.* 2009). These instruments are triggered so that only the mainshock was recorded by all the stations, and only the strongest aftershocks were recorded at some of them. At the end of 2007 November, a temporary seismic network was deployed in the focal area by the German Task Force of GFZ (Sobiesiak *et al.* 2008), in collaboration with IPGP and ENS in France, and DGF in Chile. The network was composed of 20 short period, 4 broadband and 10 strong motion stations. This network recorded several months of aftershocks between the end of 2007 November and 2008 May but only the largest aftershocks have been relocated so far.

Recently, Lancieri *et al.* (2009) and Ruiz *et al.* (2009) relocated the main aftershocks of the Tocopilla earthquake using the continuous accelerometric data from the IPOC network. These data shows that in the Northern part of the source area aftershocks were located very closely to the Chilean coastline, but that in the Southern end, aftershocks extended oceanwards of the Mejillones Peninsula.

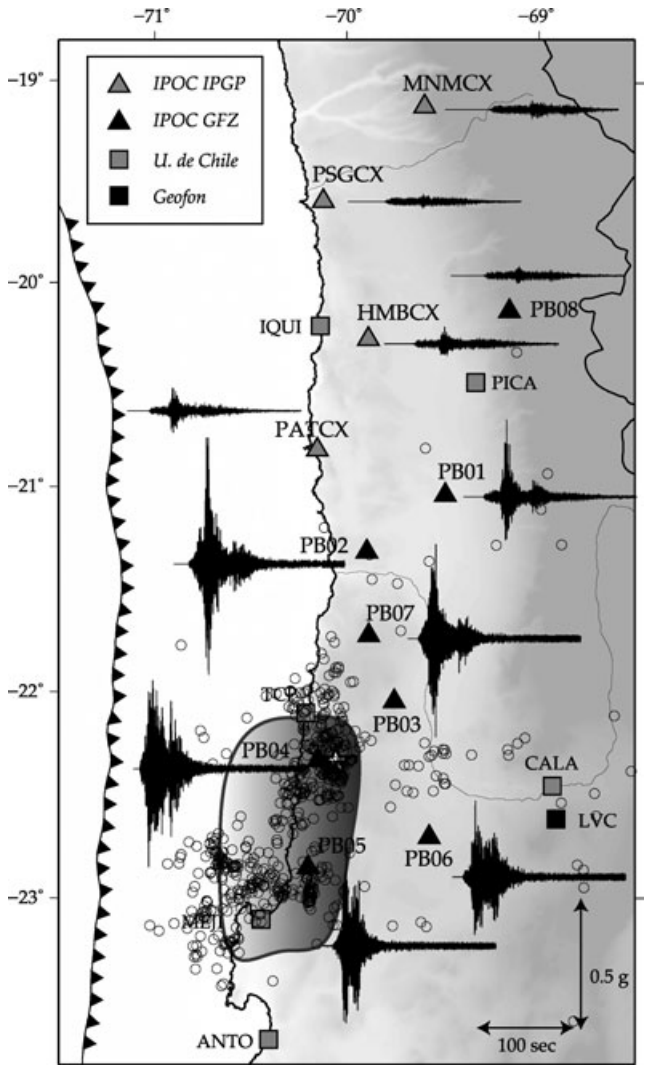

Figure 2. Star: Epicentral location of the mainshock. International Plate Boundary Observatory: Permanent accelerometers and broad-band network installed by IPGP (grey triangles) and GFZ (black triangles). Triggered strong-motion stations of the Universidad de Chile (grey squares). Geofon stations (black triangles). The data are EW accelerograms for the IPOC stations. The open circles are aftershocks relocated by Lancieri *et al.* (2009) and Ruiz *et al.* (2009) using data from DGF and IPOC.

3.2 Strong-motion data processing

The strong-motion records have absolute time and high dynamic range so that they can be used to do a detailed kinematic inversion of the rupture process. Unfortunately, these data may be contaminated by several factors, due to the installation, quality of coupling to the ground and rotational motion. These problems can affect the low frequency response of the records, so that the recovery of static displacements from strong-motion records can not be performed directly (Graizer 1979). The usual solution consists in low-pass filtering the strong-motion records at frequencies lower than the duration of the signal, but this procedure may eliminate some of the information contained in near source stations. The loss of low-frequency information is often due to an incorrect determination of the baseline that may sometimes be removed. Unfortunately, there is no universal correction scheme that can be applied to records and it may be difficult in practice (Iwan *et al.* 1985; Boore 2001; Boore & Bommer 2005). The baseline correction consists in subtracting a polynomial (Graizer 1979) or multiple linear segments (Iwan *et al.* 1985) from the acceleration records. Baseline errors produce small effects in the acceleration records, but they may significantly affect velocities and displacements obtained by integration of acceleration time series (see, also Peyrat & Favreau 2010). We adopted the following procedure to correct the baseline of the acceleration records. First, we identified constant baselines before and after the earthquake signal; then a tilted line segment was adjusted between the constant baselines by minimizing the residual average velocity at the end of the signal. This baseline correction is expected to remove a large part of any spurious low-frequency signal. We performed this baseline removal only on the stations that were clearly affected by baseline perturbations. To test our baseline correction method, we verified that low pass filtering at periods much longer than the duration of the signal (100 s) did not affect significantly the velocities thus obtained. In the last step of the process, velocities were low-pass filtered at frequencies less than 0.01 Hz with a one pass fourth-order Butterworth filter and high-pass filtered at frequencies higher than 0.1 Hz with a two pass second-order Butterworth filter for the mainshock. The aftershock data were filtered with the same type of filter, velocities were low-pass filtered at frequencies less than 0.04 Hz with a one pass fourth-order Butterworth filter and high-pass filtered at frequencies higher than 0.25 Hz with a two pass second-order Butterworth filter. The records were finally integrated to ground displacements.

3.3 Earthquake locations

The near source broad-band records of the main shock were clipped but the strong-motion data could be used to determine *P* and *S* arrival times at all available accelerometers that had good time control. We used the *Hypoinverse* (Klein 1989) program to do the location using 1-D velocity model listed in Table 2. This model was inferred from the inversion of data from the CINCA experiment reported by Husen *et al.* (1999). The main shock and three of the largest aftershocks were located in this way, their locations are listed in Table 3.

For the mainshock, we could clearly identify a couple of subevents in the strong-motion data. Two clear *S*-waves arrivals were identified (Fig. 3) confirming preliminary far-field studies that reported that the Tocopilla earthquake was a doublet and the recent work by Delouis *et al.* (2009). With these data we determined that the second subevent occurred South of the main shock about 23 s later, at a distance of 49 km and an azimuth of 175° (Fig. 4). The second source could be located only with *S* waves because *P* waves from the second event were covered by the arrival of much stronger *S* waves radiated by the main shock hypocentre. The hypocentral depth of the mainshock, 52 km, corresponds well with the lower limit of the strongly coupled seismic zone determined in this region by Tichelaar & Ruff (1991). Two aftershocks with $M_w = 6.3$ and 6.8 occurred the day after the mainshock within a few minutes of each other (Table 3). These aftershocks have similar focal mechanisms and occurred at a 3 min interval almost at the same location west of the Mejillones Peninsula. We determined depths of 40 km for the first aftershock and 28 km for the second one. Depth control for these off-shore events is unfortunately very poor because all the stations are inland. On 2007 December 16 the largest aftershock occurred near the end of the rupture zone of the main event at a depth of 49 km (see Table 3 for the location).

Table 2. Crustal models used to locate earthquakes and to generate synthetic seismograms (simplified from Husen *et al.* 1999).

	Husen *et al*. 1999 model		Simplified model		
Depth (km)	V_p (km s^{-1})	V_s (km s^{-1})	V_p (km s^{-1})	V_s (km s^{-1})	Density (g cm^{-3})
0	5.20	3.00	5.30	3.10	2.5
2	5.40	3.10			
4	5.55	3.20	5.30	3.10	2.5
6	5.70	3.30			
8	5.90	3.40			
10	6.00	3.45	6.00	3.45	2.7
15	6.80	3.80	6.90	3.95	2.8
20	6.80	3.87			
25	6.95	3.95			
30	7.00	4.05			
35	7.10	4.10			
40	7.40	4.20	7.60	4.40	3.3
45	7.70	4.35			
50	8.05	4.45			
60	8.45	4.80	8.45	4.80	3.4

Table 3. Event locations using the velocity model of Husen *et al.* (1999).

Date	Time	Lon. (°)	Lat. (°)	Depth (km)
2007/11/14	15:40:49.99	−70.06	−22.34	51.8
2007/11/14	15:41:13.75	−70.02	−22.78	47.5
2007/11/15	15:03:06.62	−70.61	−22.95	39.3
2007/11/15	15:05:57.74	−70.59	−22.98	27.7
2007/12/16	08:09:16.53	−70.22	−22.97	49.1[a]
	08:09:16.68	−70.23	−22.97	47.8[b]

[a]Using strong-motion data from the permanent network,
[b]Using strong-motion data from the permanent network and data from the aftershock network deployed by the German task force of GFZ.

3.4 Focal mechanisms

The focal mechanism and the source time history were determined using teleseismic waveform inversion with data provided by the IRIS and Geoscope data centres. Only stations at epicentral distances between 30° and 90° for the *P* waves, and between 34° and 87° for *SH* waves, were used to avoid multipathing, upper mantle and core arrivals. Source parameters were determined using the inversion method of Nábělek (1984), assuming a double-couple point source. At the source, the velocity structure of Table 2 was assumed, while a homogeneous half-space was assumed at the receivers, with $v_p = 6.4$ km s^{-1}, $v_s = 3.7$ km s^{-1}, $\rho = 2.8$ g cm^{-3}. The displacement records were finally bandpass filtered from 0.01 to 1 Hz using a three-pole Butterworth filter to avoid the effect of unmodelled small-scale structures. For the main event we inverted the broadband records assuming the presence of two sources separated by 23 s, at a distance of 49 km and in the 175°E azimuth.

The azimuthal distribution of stations (Fig. 5) constrained very well the dip of the vertical nodal plane, but left a large trade-off between strike and rake of the shallow dipping plane, as it is often the case for teleseismic inversion of earthquakes in Chile. This is mainly due to a poor distribution of seismic stations in the Pacific. For the main event we found that the strike was 358°, the dip angle 26° and the rake 109° (see also Table 4), this mechanism corresponds very well with the direction of oblique convergence in Northern Chile. The source time function contained two pulses with a total duration of 38 s. Although there is still some uncertainty in the determination of the dip angle, it agrees with the previous studies who showed that the slab dips range from an angle of approximately 30° (Araujo & Suárez 1994) to an angle of 21° (Buske *et al.* 2002) in the region

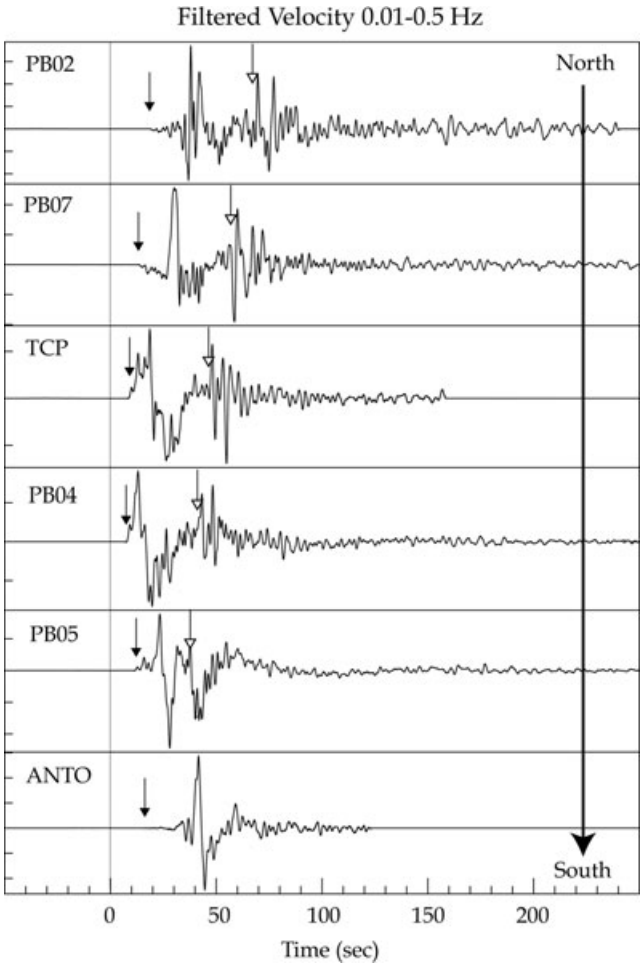

Figure 3. Acceleration (vertical component) records integrated to velocity and filtered between 0.01 and 0.5 Hz. Stations are plotted from north to south (see Fig. 2 for locations). Black arrows correspond to *P* -wave arrivals for the mainshock and white-headed arrows correspond to *S*-wave arrivals from the second source.

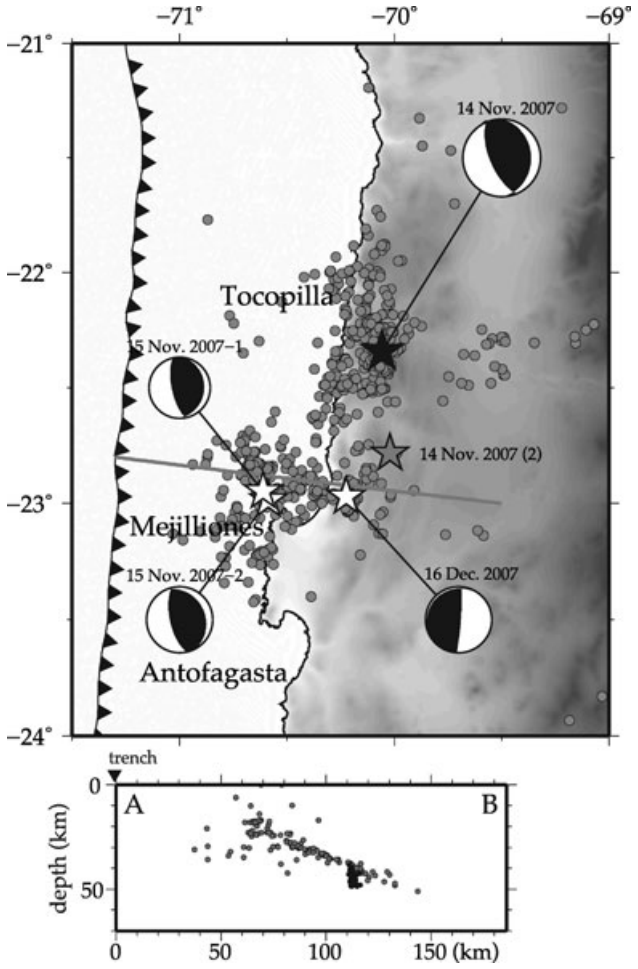

Figure 4. Top: Location of the two subevents of the Tocopilla earthquake (black and grey stars), and the locations of the main aftershocks (white stars). Local seismicity and aftershocks were relocated by Lancieri *et al.* (2009) using IPOC data. The aftershock data covers the period from 2007 November 14 until the end of 2007 November (grey dots). Bottom: West–east cross section of the aftershocks located by the above authors (grey dots) and together with the aftershocks of the 2007 December 16 event located by Ruiz *et al.* (2009) (black dots).

between 21°S and 24°S. These results are largely in agreement with those of (Delouis *et al.* 2009).

The fault plane solution we found for the aftershock of 2007 November 15 (Fig. 6; Table 4) has a strike of about 332°, a dip angle of 24° and a rake of 76°. This is in very good agreement with the direction of the oblique convergence, but the dip indicates a slightly shallower fault plane than the mainshock. The source time function was found to be a simple pulse with a total duration of 12 s. The fault plane of the large slab-push aftershock of 2007 December 16 (Fig. 7; Table 4) had a strike of about 4°, a steep dip angle of 85° and a rake of 83°. The source time function was a simple pulse with a duration of only 4 s. In Fig. 4, we plot with dark dots the aftershocks of the slab-push event of 2007 December 16 relocated by Ruiz *et al.* (2009). They are clearly aligned in a subvertical direction indicating that this event broke the slab almost vertically.

4 DETAILED KINEMATIC SOURCE STUDY

We determined the detailed source process of the Tocopilla earthquake and of its main aftershocks independently using teleseismic and strong-motion data. We use a classical inversion method based on rectangular patches for the inversion of teleseismic data and an elliptical patch approximation for the near-field data. We verify that the model obtained with near-field data is compatible with the teleseismic data. The reason we use the elliptical patch approximation for modelling near-field data is that our stations are about 50 km apart, so that they do not have enough spatial resolving power to use the more usual rectangular patch approximation. The elliptical patch approximation is designed so that we determine the dominant features of the source model.

4.1 Teleseismic inversion

We used the method of Kikuchi & Kanamori (1991) to investigate the rupture process from teleseismic body waves. We performed a number of tests using different fault dimensions, grid sampling, rupture velocity and hypocentral depths. Initially, we did the inversion allowing for changes in the fault orientation, but in a second step we determined only the slip distribution.

We modelled 18 vertical components *P* wave and 11 *SH*-wave displacement records with good azimuthal coverage at teleseismic distances. A window of 90 s was used for the inversion. The instrument responses were removed and the data integrated into displacement and bandpass filtered between 0.01 and 1 Hz. Synthetic Green functions were computed using a simplified crustal velocity model for the region listed in Table 2. The fault plane solution is consistent with that listed in Table 4, which was determined using a two point source model using the method of Nábělek (1984). The best kinematic inversion was obtained for the shallow dipping fault plane (dip = 26°). We then divided the fault surface into square grids of 20 km spacing with a total area of 160 km × 80 km. The best solution is shown in Fig. 8. In the kinematic inversion, we only inverted for the slip distribution, assuming that rupture started from the hypocentre situated at 50 km and propagated radially with fixed rupture velocity of 2.7 km s^{-1}. We acknowledge though, that there is little control on the rupture speed with these low pass filtered far-field data. The total seismic moment determined from the far-field data inversion was $M_0 = 2.9 \times 10^{20}$ N m ($M_w = 7.6$). The duration of the integrated moment rate function was 40 s.

The kinematic inversion of the far field data confirms that the Tocopilla earthquake was a double event with two subevents of roughly the same mechanism, the second shock was located some 50 km from the first event, as observed directly on the strong-motion records (Section 3.3). This is in very good agreement with the locations determined from integrated near-field data. The overall dimensions of the rupture zone was found to be 150 × 60 km, with the rupture propagating in a N–S direction. The maximum slip was determined as 1.5 m. Fig. 8 shows the fit between observed and predicted waveforms and the slip distribution over the fault. As in the previous work by Delouis *et al.* (2009), we find a slip distribution with two patches elongated in the N–S direction.

4.2 Kinematic inversion using near-field strong-motion data

As already mentioned, the Tocopilla earthquake occurred under the IPOC strong-motion network. It was also very well recorded by the triggered strong-motion network operated by the University of Chile. These records have absolute time and high dynamic range so that they can be used to do a kinematic inversion of the rupture process.

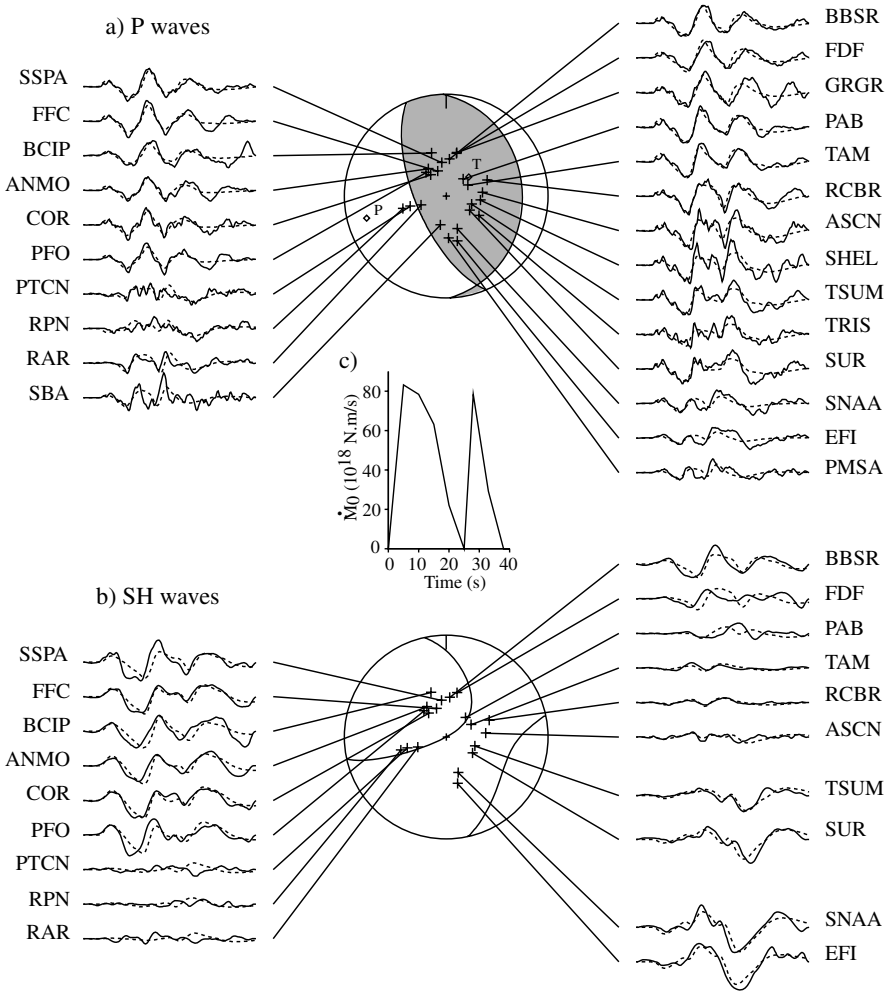

Figure 5. Far field body wave inversion of the mainshock of 2007 November 14: focal mechanism obtained by inversion using the method of Nábělek (1984). Observed (solid lines) and synthetic (dashed lines) for (a) *P*-displacements waveforms and (b) *SH*-displacement waveforms, with (c) the time source function.

Table 4. Focal mechanisms determined by teleseismic inversion.

Date	Strike (°)	Dip (°)	Rake (°)	Duration (s)
2007/11/14	358	26	109	38
2007/11/15	332	24	76	12
2007/12/16	4	85	83	4

Past experiences show that to obtain a reliable image of the source process, many conditions are required: a good density and coverage of the strong-motion data, small distances from the source to reduce multipathing, good quality of records and a good knowledge of the velocity model. The parameterization of the source model must be consistent the intrinsic possibilities of the seismic array and meaningful for the source process itself (Hartzell *et al.* 2007).

We believe that an elliptical patch approximation is adequate for situations like Northern Chile where the station locations are roughly 50 km apart and the velocity structure is not known in enough detail. This parameterization has the advantage that it produces an image of the source made of asperity-like patches. Elliptical patch parameterization was introduced by Vallée & Bouchon (2004) to model far-field waveforms for teleseismic events. The application of the method to near-field strong-motion kinematic inversion and its resolution was discussed in additional detail by Peyrat & Favreau (2010) and Di Carli *et al.* (2008).

4.2.1 Description of the forward problem

In the forward model, for each elliptical patch we adopted the slip distribution produced by a simple elliptical crack. Such a slip patch is determined by six parameters: two coordinates for its centre, the angle of orientation of the ellipse, its two semi-major axes and the peak value of slip at the centre of the ellipse. The mechanism is assumed to be uniform over the whole fault. The rupture is assumed to develop radially from hypocentre, propagating at constant rupture speed. In kinematic inversion, we also have to define the local source time function. Although we are aware that dynamic source models show that source time functions are usually complex, here we used a simple triangular slip rate time function of 3 s of duration. We also performed inversions with variable rupture velocities and rise times presented in the Supporting Information.

From the teleseismic inversion, we can assume that the shortest source duration was almost 10 s (second source in Fig. 8b). Because the total duration of the rupture process is of the order of 40 s, our near-field data should resolve well source features of the order of this period (10 s, or 4.5 km for *S* waves). For this reason, we chose to perform a low-frequency inversion from 0.01 to 0.1 Hz. This frequency range contains most of the energy of the displacement waveforms and enough details to determine the main features of the source. To test the reliability of our low-frequency inversion, we also performed the inversion in the 0.01–0.25 Hz frequency band.

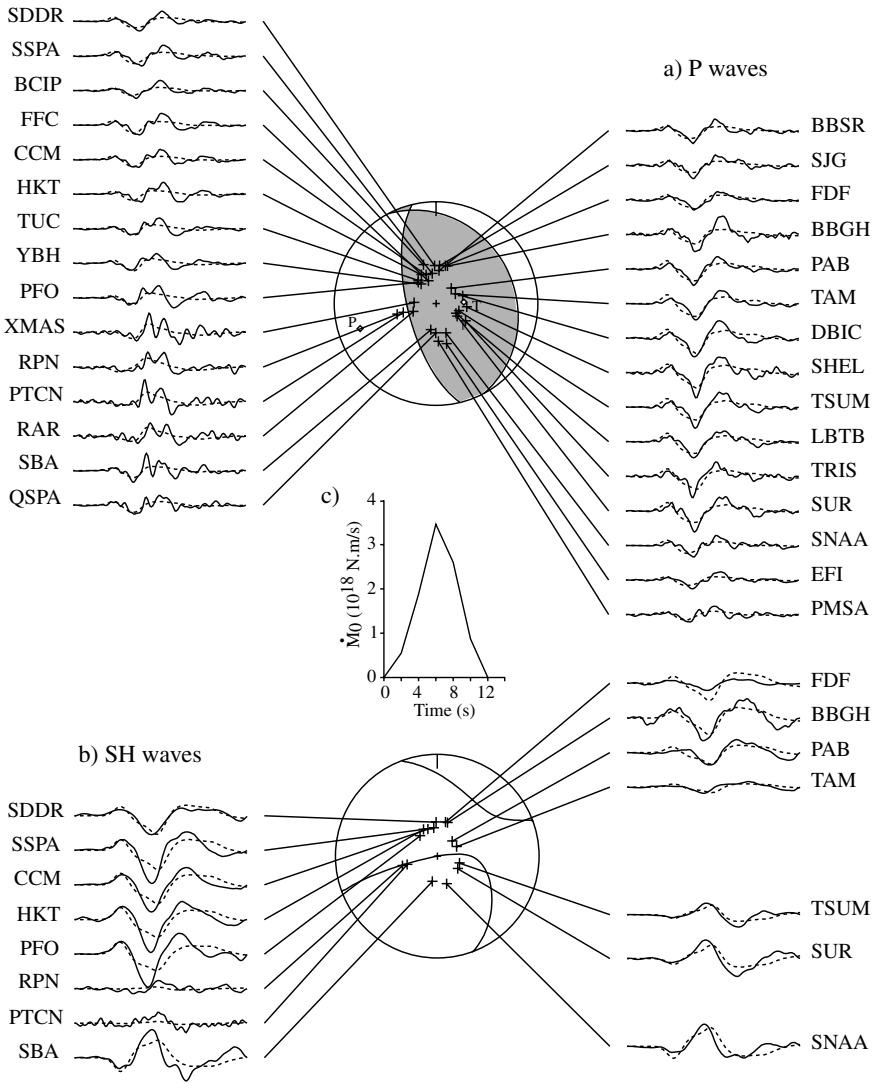

Figure 6. Main aftershock of 2007 November 15: focal mechanism obtained by teleseismic body-wave inversion. Observed (solid lines) and synthetic (dashed lines) for (a) *P*-displacements waveforms and (b) *SH*-displacement waveforms, with (c) the time source function.

The results are shown in the Supporting Information. We realize that even in our low-frequency approach we could not uniquely determine a source model.

Once the slip distribution is defined in the forward problem, we compute synthetic seismograms using the spectral discrete wave number integration method developed by Bouchon (1981) and implemented in AXITRA program of Coutant (1990). For the structure we used the same layered model as we used for the far field simulations (Table 2, simplified model).

4.2.2 Solution of the inverse problem for the main event

For the inversion we used a systematic, fully non-linear inversion method based on the Neighbourhood algorithm (NA) developed by Sambridge (1999a). The cost function

$$\chi = \frac{\int_0^T (\text{synth} - \text{obs})^2 \mathrm{d}t}{\int_0^T (\text{obs})^2 \mathrm{d}t} \quad (1)$$

was the normalized L_2 norm of the difference between synthetics and observed seismograms. The data and synthetics were corrected displacement waveforms and filtered in the same way.

For the main shock, inspired by the broadband far-field modelling, we decided to invert a source model consisting of two elliptical slip patches that ruptured at constant speed starting from the hypocentre. The model space for this problem has 14 independent parameters, seven for each elliptical patch. We could have added two more parameters if we had been able to resolve the rise time, but this was not possible because our data can not resolve periods less than 4 s. For this reason, we fixed the rise time at 3 s for each patch.

The result of the kinematic inversion of the main Tocopilla earthquake, shown in Fig. 9(a), presents two well-defined slip patches elongated in a roughly north–south direction. Rupture started almost right below the PB04 strong-motion station and propagated bilaterally at a constant speed of 2.4 km s^{-1}; it then stopped just north of the city of Tocopilla, but continued to propagate southwards breaking a second asperity to the south at a constant speed of 2.7 km s^{-1}. The mean rupture velocity is about 2.65 km s^{-1}, lower than the fixed value of the teleseismic inversion. The first asperity has a maximum slip of 2.6 m and the second one 2.4 m. The total seismic moment is 3.68×10^{20} N m, $M_w = 7.6$. This will be called source model A.

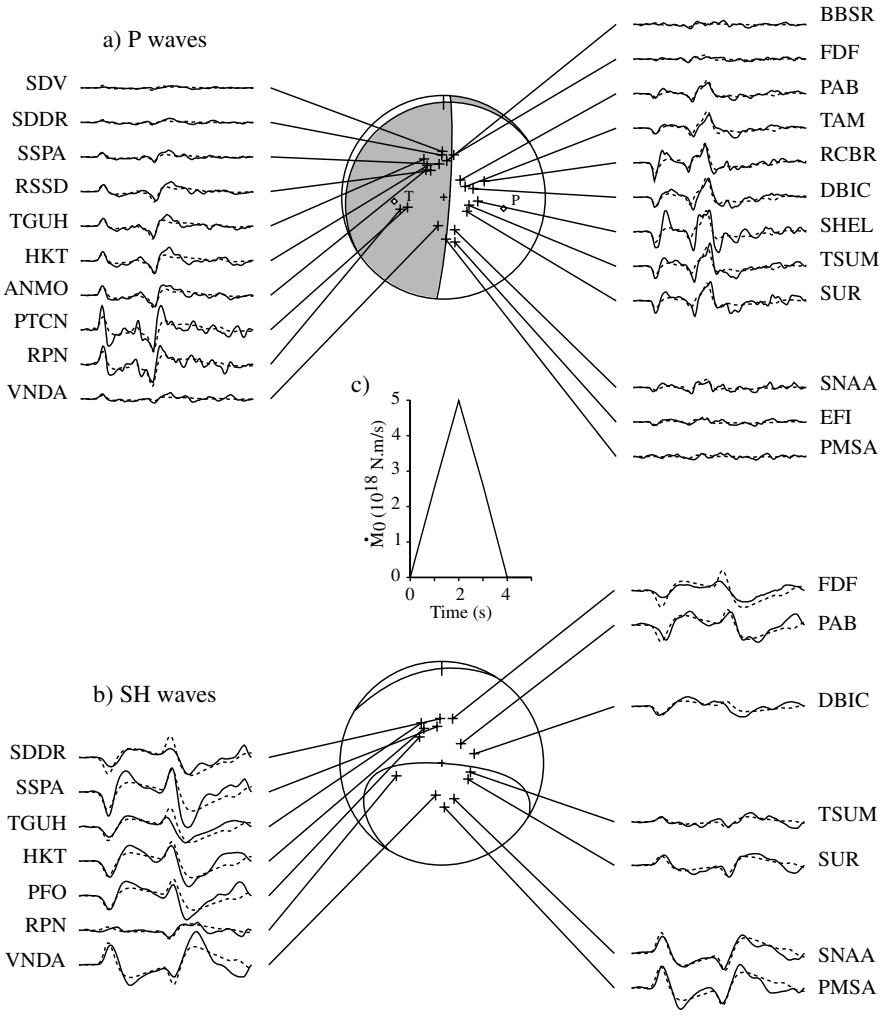

Figure 7. Large slab-push aftershock of 2007 December 16: focal mechanism obtained by teleseismic body-wave inversion. Observed (solid lines) and synthetic (dashed lines) for (a) *P*-displacements waveforms and (b) *SH*-displacement waveforms, with (c) the time source function.

As we had previously located the hypocentre of the second subevent from high-frequency accelerometric data, we also inverted for two subevents, each with its own fixed hypocentre. The result of this second inversion, model B, is shown in Fig. 9(b). The first asperity has a maximum slip of 2.4 m and the second one 3.8 m. The total seismic moment is 3.18×10^{20} N m, $M_w = 7.6$. The rupture velocities for the two subevents are, respectively, 2.2 and 5 km s^{-1}. Thus, the propagation inside the first asperity is subshear, whereas rupture propagation in the second asperity is locally supershear. We consider that we do not have enough seismic data to prove that rupture was actually supershear, so that we consider model B less likely than model A. However, the local supershear velocity can be explained by a change in the rupture direction for the second subevent. For the first subevent, rupture propagates almost perpendicular to the direction of slip like an anti-plane (mode III) shear crack. But for the second subevent, rupture propagates almost in the direction of slip, like an in-plane (mode II) shear crack for which cracks may propagate at supershear rupture speeds. Let us remark that the average rupture velocity is 2.65 km s^{-1}, like for model A. The first asperity of Model B is similar to that of Model A of Fig. 9(a), but the second asperity is quite different. Fig. 9(a–b) shows these two end models of a set of possible models. Although they differ in details that may only be resolved by a denser accelerometer network, the overall features of the two sources are similar. They also agree quite well with the slip distribution obtained with teleseismic inversion (Fig. 9c) where the maximum slip is lower but the distribution is stretched and the waveform fit are good and indistinguishable for the 2 models (Fig. 10). Additional tests of the inversion results are presented in Supporting Information.

To complete our study of the source, we also computed synthetics for models A and B at teleseismic distances. The synthetic generated in this way are compared with the data used in the teleseismic inversion in Fig. 11. The good agreement between synthetics and observed data indicate that our near-field models agree also with the teleseismic data.

The convergence of the parameters is an indicator of the solution reliability. In Fig. 12, we plot the evolution of the inverted parameters as a function of iteration number in the NA algorithm. The grey colour scale indicates the level of misfit. Models A and B shows similar convergence. We observe that enough models are generated to obtain a stable unique branch of solution, with reasonable fluctuations compared to the intervals of search.

We conclude that the Tocopilla earthquake ruptured the interplate seismic zone over more than 130 km The main shock started near the Northern end of the rupture zone, below the PB04 accelerometer, some 20 km SE of Tocopilla. Rupture propagated mainly southward

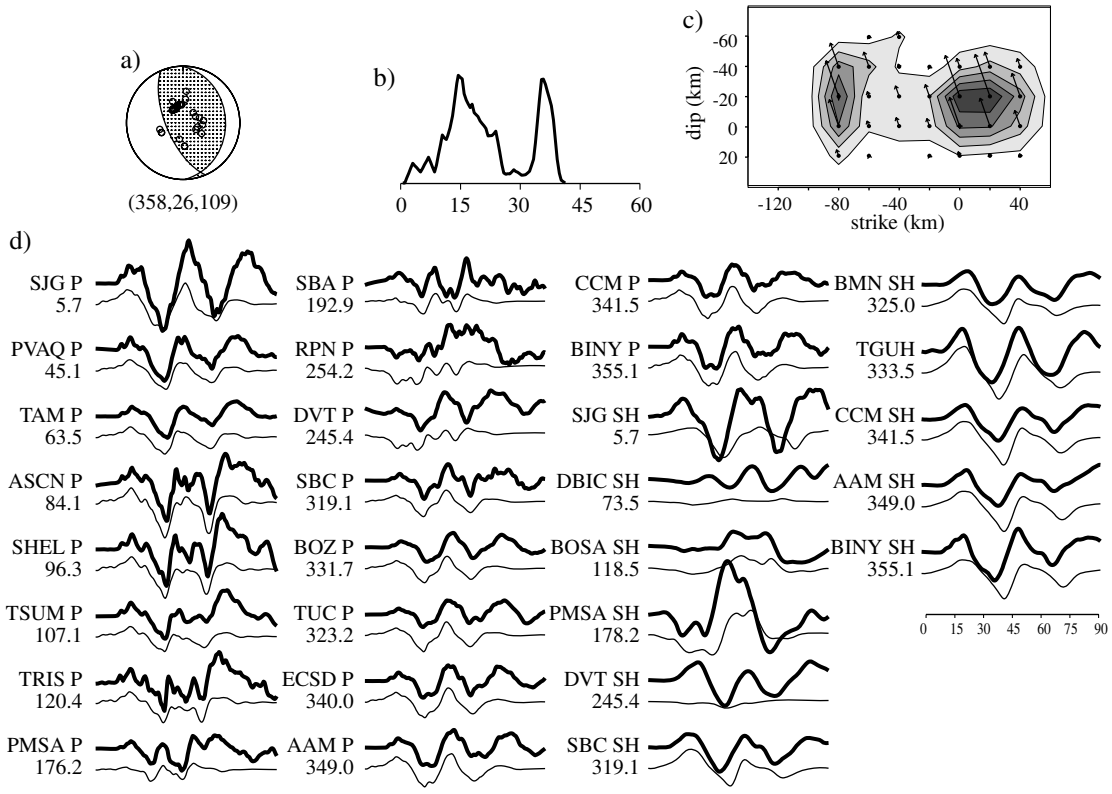

Figure 8. Teleseismic extended source inversion of the Tocopilla mainshock of 2007 November 14: (a) focal mechanism; (b) source time function; (c) slip distribution (maximum is 1.5 m) and (d) waveforms fit, observed (thick lines) and synthetic (thin lines) displacements.

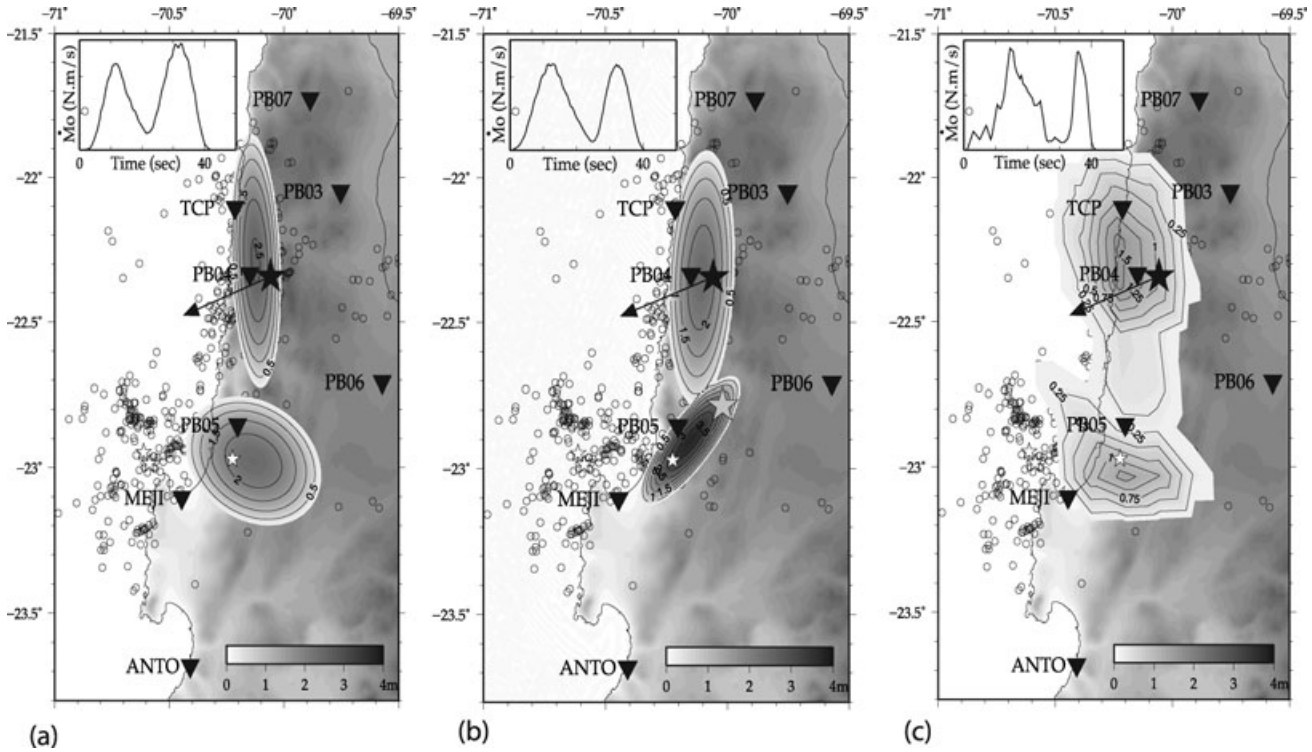

Figure 9. Near-field inversion of the Tocopilla earthquake of 2007 November 14. (a, b) Slip distributions from inversion of near-field displacements obtained by integration of the strong-motion data filtered in the 0.01–0.1 Hz band. Line contours plotted every 0.5 m. Insets show the moment rate functions obtained from strong-motion inversion. Black star is the hypocentre, grey star the second source, smaller white stars are the main aftershocks. Black arrow is the rake direction. (a) Inversion of two elliptical patches with rupture propagating circularly from the hypocentre of the main event. (b) Inversion with two elliptical patches. Rupture propagation starts from the hypocentre for the first asperity and from the location of the second asperity determined from high frequency data. (c) Slip distribution obtained by teleseismic inversion (same as Fig. 8c), line contours plotted every 0.25 m.

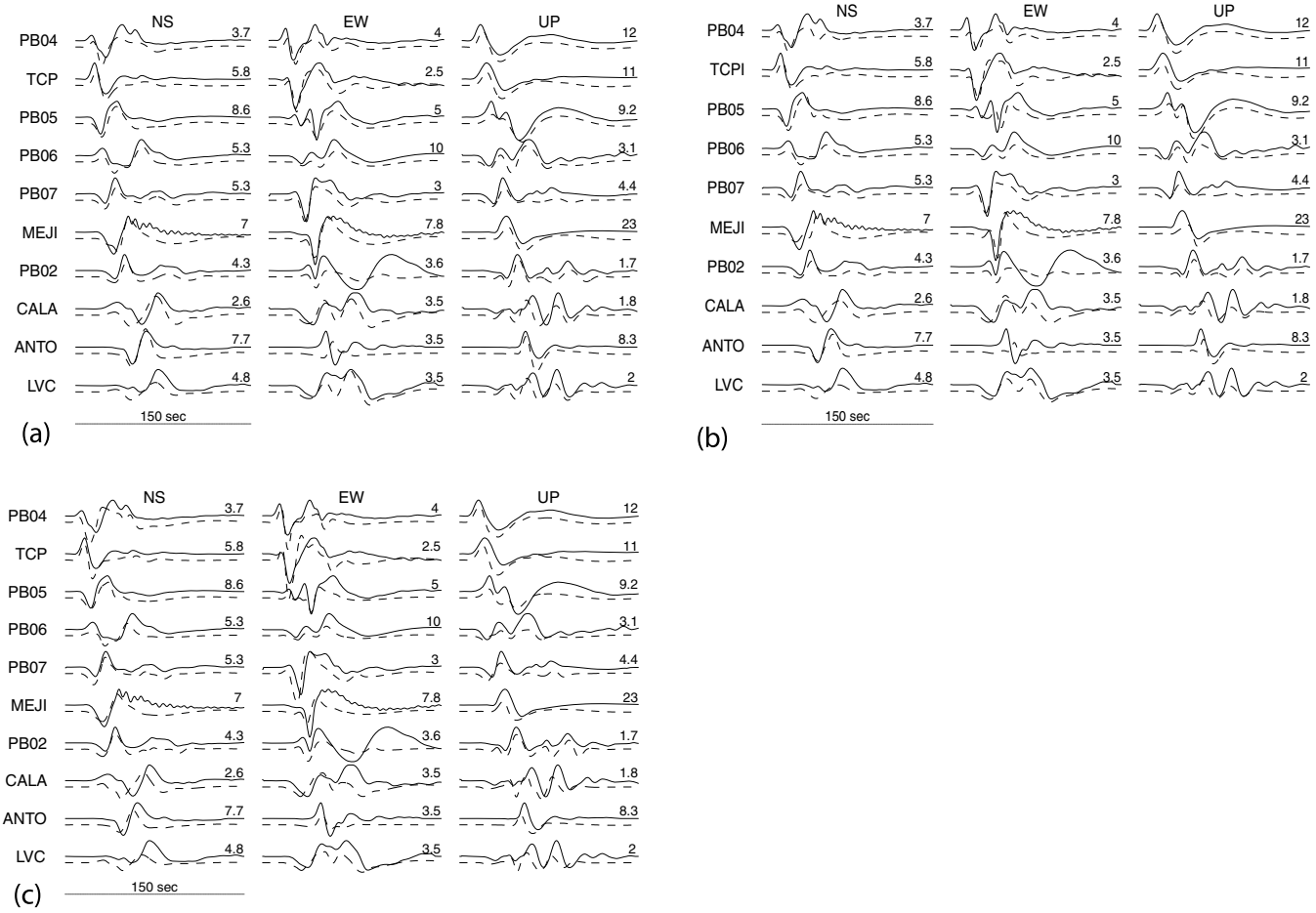

Figure 10. Near-field inversion of the Tocopilla earthquake of 2007 November 14. Strong-motion waveforms: acceleration is integrated into displacement and filtered between 0.01 and 0.1 Hz, number right to each trace is the maximum value (cm): observed (solid line) and synthetic (dashed line) for (a–b) direct model from slip distribution obtained with strong-motion inversion, models from Figs 9a–b, and (c) forward model using the slip distribution obtained by the teleseismic inversion (Fig. 9c). The relative misfit values are $\text{rms}_a = 0.5$, $\text{rms}_b = 0.57$ and $\text{rms}_c = 0.7$.

with a clearly identified second event that started about 23 s after the main shock and was located 47–49 km south from the hypocentre. The network configuration resolves well the slip distribution along the strike of the Chilean subduction zone, but does a much worse job in identifying the slip distribution in the E–W direction. In spite of this difficulty, we believe that we have identified the main aspects of the complex source process that gave rise to the Tocopilla earthquake. The inversion of the main event is in excellent agreement with the aftershock distribution determined by Lancieri *et al.* (2009) who showed that most of the early aftershocks of the main event were located on a band about 40 km wide along the coast of Northern Chile.

In a companion work Béjar-Pizarro *et al.* (2010), inverted interferometric data and velocity vectors and locations of the largest aftershocks, as well as the occurrence of the slab-push event of December located inside the subducted slab. Their models confirm the north–south extent of the rupture process. They found evidence for at least two main distinct slip patches along the strike, but they suffer from the same lack of resolution in the E–W direction as we did.

4.3 Analysis of uncertainty of the inverted kinematic models

After inversion we studied the resolving power of the inversion method using the bayesian neighbourhood algorithm (NA-bayes or NAB) of Sambridge (1999b). This technique has already been used for kinematic rupture inversion with strong-motion data by Monelli & Mai (2008) and Peyrat & Favreau (2010). The NAB algorithm uses the set of models generated during the NA search stage (inversion) to estimate resolution and possible trade-offs, within a bayesian framework. From this point of view the solution to the inverse problem is the posterior probability density function (PDF) computed for each parameter. The main advantage of NAB is to approximate the marginal PDF without the need of running the forward simulation for each resampled model.

Following Sambridge (1999b), the marginal PDF can be written as

$$P(m) = A \exp\left(-\frac{1}{2}\left(\frac{|d(m) - \text{obs}|_{L_2}}{\epsilon |\text{obs}|_{L_2}}\right)^2\right), \quad (2)$$

where, $d(m)$ are the synthetics computed for model m, obs are the observed seismograms, A is a normalization factor and ϵ a is the *a priori* variance of the (supposedly Gaussian) noise in the observed data. Strong-motion data exhibit several sources of uncertainty, including random and non-random perturbations like the piecewise linear baseline correction needed to compute displacement waveforms from accelerograms. We have partly corrected this systematic bias. However, to stay conservative, we chose $\epsilon = 0.1$. This corresponds to a confidence of 90 per cent in the observed data.

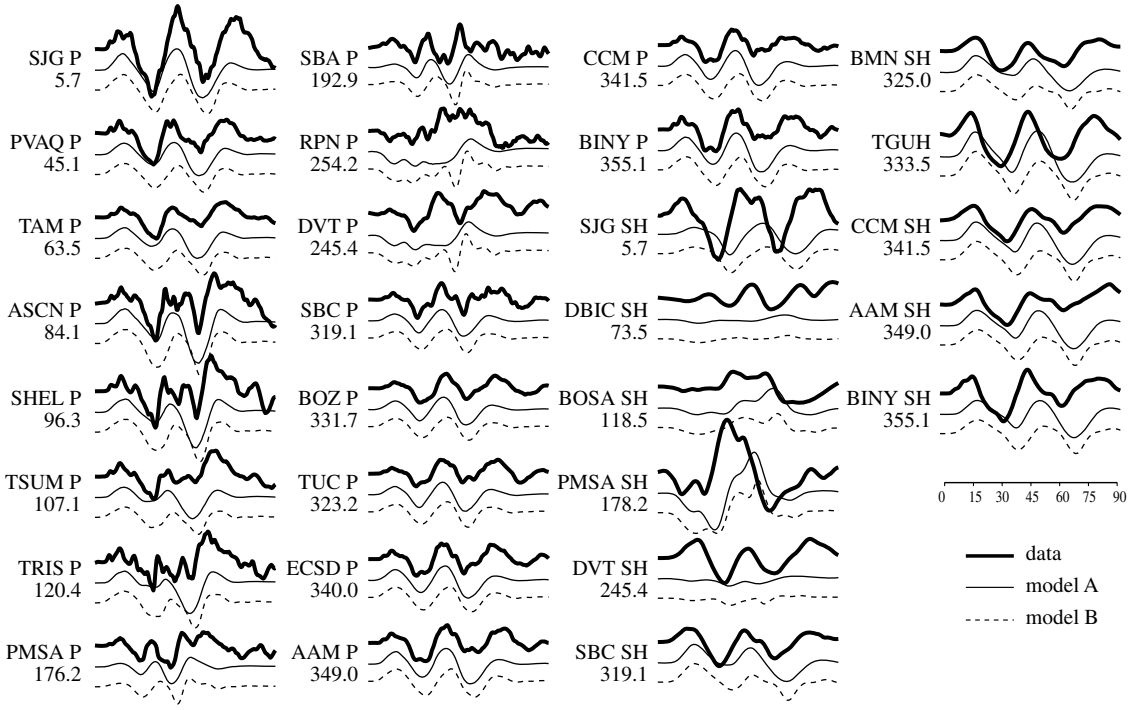

Figure 11. Inversion of the Tocopilla earthquake of 2007 November 14. Synthetics generated for kinematic models A (thin lines) and B (dashed lines) are compared to teleseismic data (thick lines) and synthetic (thin lines) displacements.

We computed for each model parameter the marginal PDFs which are shown in Fig. 13 for each inverted parameter and for several inferred parameters like the surface of the two patches (s_1 and s_2), the total seismic moment (M_o), the approximated rupture time of the first patch (t_{r1}) and the coordinates of the centroid on the fault (x_c towards strike and y_c towards dip). The marginals provide a useful way of testing how the sampled algorithm converges.

The final models (vertical bars in Fig. 13) correspond for most of the parameters to the marginal PDF peaks, indicating an acceptable convergence of the previous NA algorithm. The width of the marginals is an indicator of the confidence that may be placed on each parameter: the narrower the distribution, the better resolved is the parameter. Note that the marginal PDF for each parameter does not follow the same distribution for each model, and they do not always have a Gaussian shape. The only marginals with Gaussian shape correspond to slip, rupture velocities, moment, rupture time, centroid position and patch positions. For the other parameters, the skewed distributions are probably due to the limitations of the parameter space; another explanation is that some parameters are correlated, like the sizes (a and b) of the patches. Indeed, the surfaces of the patches are better constrained.

The marginal distributions show that all these models share some large-scale features. As expected, seismic moment and centroid are well constrained and consistent. Likewise, surface (s_1), position (r_h,α_h), slip ($slip_1$), approximate rupture time of the first slip patch ($t_{r1} = \sqrt{a_1 b_1}/v_r$), are constrained and consistent, although a slip-surface trade-off is visible. We make the same remarks for the second patch, to conclude that much better resolution is achieved on the large-scale features of the models rather than on their details.

4.4 Source study of the main aftershocks

We did kinematic inversions of the rupture process of the three main aftershocks listed in Table 3 using the same methods that we used to invert for slip of the mainshock. We again inverted independently teleseismic data and the strong-motion data.

Fig. 14 shows the slip distributions obtained for the bigger aftershock of 2007 November 15 (15:05:58) using far-field and near-field data. For the inversion of the near-field data a single elliptical asperity was adopted. The results of the two separate inversions are very similar. The November 15 event started to the south–west from the mainshock (Fig. 18) and propagated further to the west into the shallower zone of the seismogenic region of the subducting slab. Maximum slip is 0.63 m and the extent of the rupture is 18 km. The total seismic moment is 2.14×10^{19} N m, $M_w = 6.8$. The data fit are shown only for the strong-motion data used for inversion in Fig. 15(a). Few minutes before that event another significant (M_w 6.3) aftershock occurred (Table 3). The slip distribution for this event is shown in Fig. 18, and is located just between the second asperity of the mainshock and the asperity of the November 15 $M_w = 6.8$ aftershock.

As mentioned earlier, the 2007 December 16 aftershock was of a very different nature than the main event and the November 15 aftershocks. This event was a slab-push event with *P*-wave polarities that almost perfectly reversed from those of the main shock. Events of this kind have been studied in central Chile by Lemoine *et al.* (2002). As shown by the aftershock distribution plotted in Fig. 4, the event started inside the slab and then propagated almost vertically downward fracturing the subducted plate. The model shown in Fig. 14 has a maxim slip of 1.97 m and a source area of 13 km × 8 km. The total seismic moment is 2.09×10^{19} N m, $M_w = 6.8$. Waveform data in Fig. 15(b) are well fitted by the model

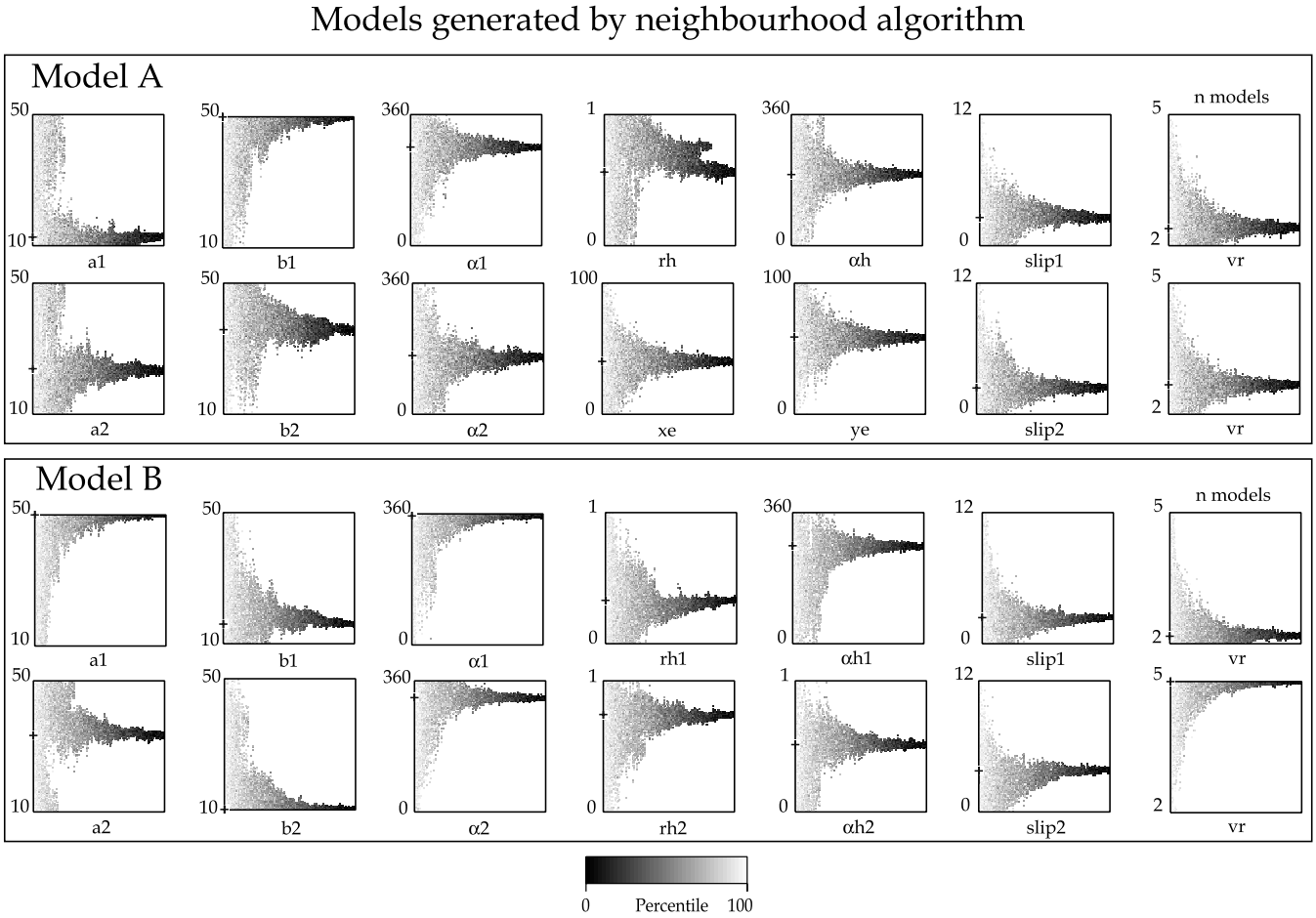

Figure 12. Inversion of the Tocopilla earthquake of 2007 November 14. Convergence of Neighbourhood algorithm for the kinematic models A and B. Each panel shows the value of an inverted parameter (vertical axis) plotted against the model number (horizontal axis). a_1, b_1, a_2 and b_2 are the lengths of the axes of the elliptic slip patches (km). α_1 and α_2 are their orientation (degree). h_r and α_h control the position of the ellipse relatively to the hypocentre. $slip_1$ and $slip_2$ are the maximal slips on each ellipse (m). v_r is the rupture velocity (km s^{-1}). x_e and y_e are the position of the centre of the second ellipse (km).

and show a much more impulsive and simple signal than for the November 15 aftershock probably due to the location of this slab-push event right below the stations.

5 COULOMB STRESS CHANGE AND TRIGGERING OF AFTERSHOCKS

We investigated stress transfer from the mainshock to its surroundings, and examined the distribution of stress on the rupture surface for the well-determined aftershocks. The December 16 event is a slab-push event that occurred in the subducting slab. It has been proposed that this compressional events occur after some large thrust events (Astiz & Kanamori 1986; Lemoine *et al.* 2002). An alternative, or complementary, explanation is that along-slab compressional events are due to stresses generated inside the Nazca plate by aseismic slip below the seismogenic zone (Gardi *et al.* 2006).

We computed changes in Coulomb stress using the Coulomb 3.1 software described by Toda *et al.* (2005) and Lin & Stein (2004). This program uses dislocation to compute stresses on receiver planes in a half-space, with uniform elastic properties. The Coulomb stress change is defined as $\Delta\mathrm{CFF} = \Delta\tau + \mu\Delta\sigma$, where $\Delta\tau$ is the change in shear stress (positive in the slip direction), $\Delta\tau$ is the change in normal stress (positive when the fault is unclamped), and μ is the apparent friction coefficient after accounting for pore fluid pressure effects. Previous studies have tested elastic properties values of the material. Here, we used reasonable values of the elastic parameters for a subduction zone (Lin & Stein 2004). Young's modulus was $E = 8 \times 10^4$ MPa, Poisson's ratio $\nu = 0.25$, and the effective coefficient of friction $\mu = 0.4$.

We used our slip models to calculate the Coulomb stress changes on the rupture plane and in its immediate vicinity. As expected, the computations reveal large stress concentrations on and off the fault. First we compute Coulomb stress change on faults with the same thrust mechanism as the largest aftershocks of the November 15, which is actually very similar to that of the mainshock. Fig. 16 shows that these two large aftershocks occur in regions where the stress increased. In the south-western end of the fault, where these events occurred, thrust faulting is promoted in the upper part of the fault above the lower edge of the source and inhibited downdip of the rupture for both models A and B. In Fig. 17, we show the Coulomb stress changes on a sub-vertical fault like that of the December 16 slab-push event. It is clear from our computations that the change in Coulomb failure stress produced by the mainshock can explain the occurrence of the December 16 earthquake for both models A and B. This event is located in a region of increased Coulomb stress, see Gardi *et al.* (2006) for a more ample discussion of the triggering of slab push events.

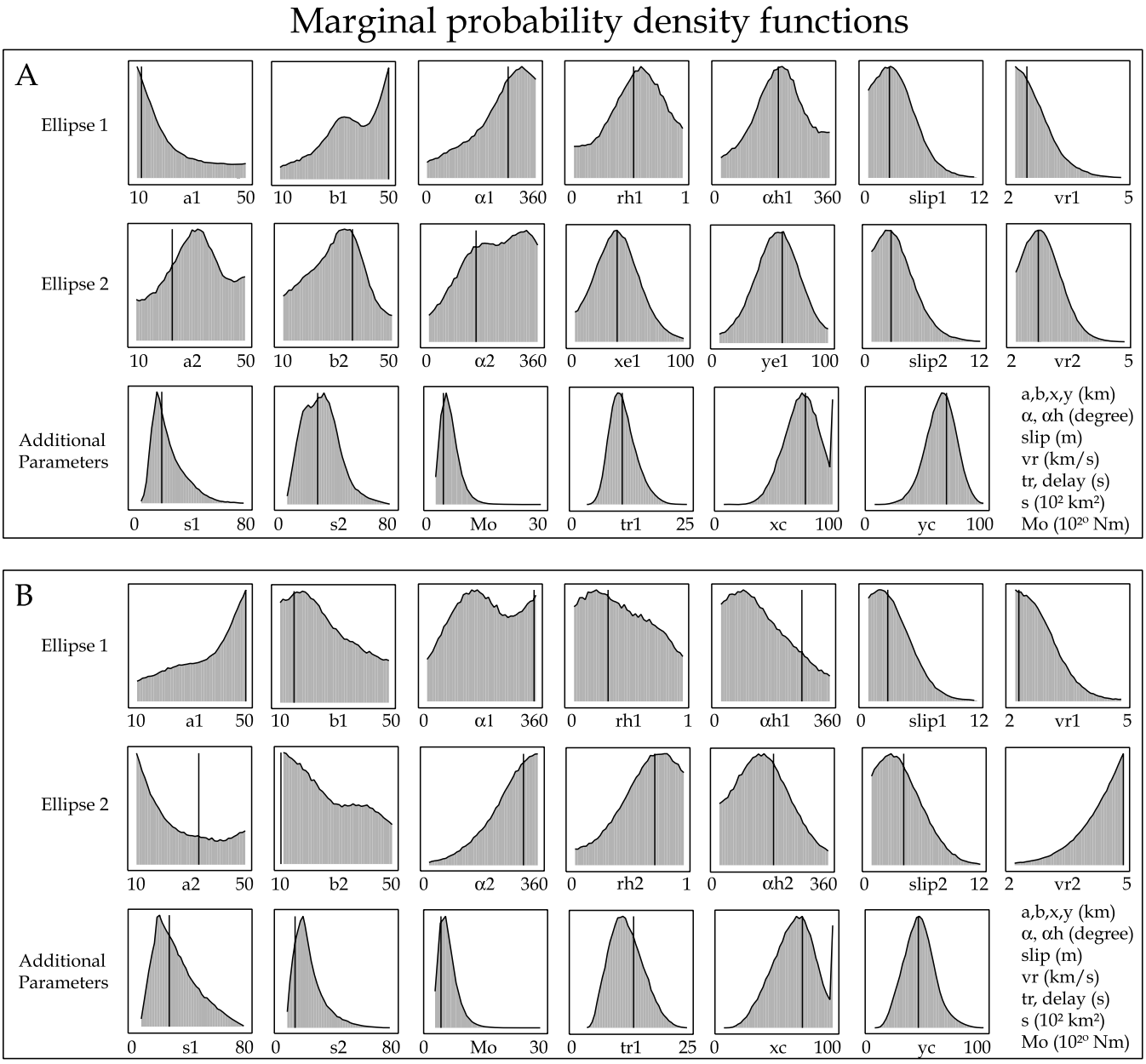

Figure 13. Near-field inversion of the Tocopilla earthquake of 2007 November 14. Results of the resampling algorithm for the two kinematic models A and B. Each panel represents the marginal PDF for the inverted parameters and for some additional deduced parameters. The first row represents the PDF of the parameters of the first slip patch, and the rupture velocity. The second row represents the PDF of the parameters of the second slip patch. The third row represents the PDF of the following additional parameters computed during the resampling: the surface of the ellipses (s_1 and s_2), the total seismic moment, the approximated rupture time on the first ellipse (t_{r1}) and the coordinates of the rupture centroid on the fault (x_c and y_c). Each x-axis is over the complete range of the parameters space. The vertical lines show the results of each model. Each curve is scaled to the same maximum height, not the same area.

6 DISCUSSION

We determined the source process of the 2007 Tocopilla earthquake and of its largest aftershocks using non-linear kinematic inversion methods. Fig. 18 shows a summary of the slip distributions of these earthquakes and a scenario of the rupture process. The mainshock was a multiple event with two major subasperities distributed roughly north–south below the coastline. Our kinematic inversion indicates that rupture stopped just North of the Mejillones peninsula, near the Northern edge of the rupture zone of the $M_w = 8$ Antofagasta earthquake of 1995 July 30. The largest aftershocks of November 15 as well as several of the smaller ones were located off the Mejillones peninsula near the Southern termination of the rupture zone. One month later, on 2007 December 16, a large aftershock of $M_w = 6.8$ occurred inside the downgoing slab just below the second asperity of the mainshock.

Although as mentioned earlier, our data does not provide enough resolution in the E–W direction, our inversion results imply that rupture occurred only on the lowermost part of the seismogenic interface between the Nazca and South American plates. This is confirmed by the relocated aftershock distribution determined by Lancieri *et al.* (2009) and Ruiz *et al.* (2009). Geodetic data studied by Béjar-Pizarro *et al.* (2010) confirm that rupture occurred near the bottom of the seismogenic zone. It appears then that only part of the

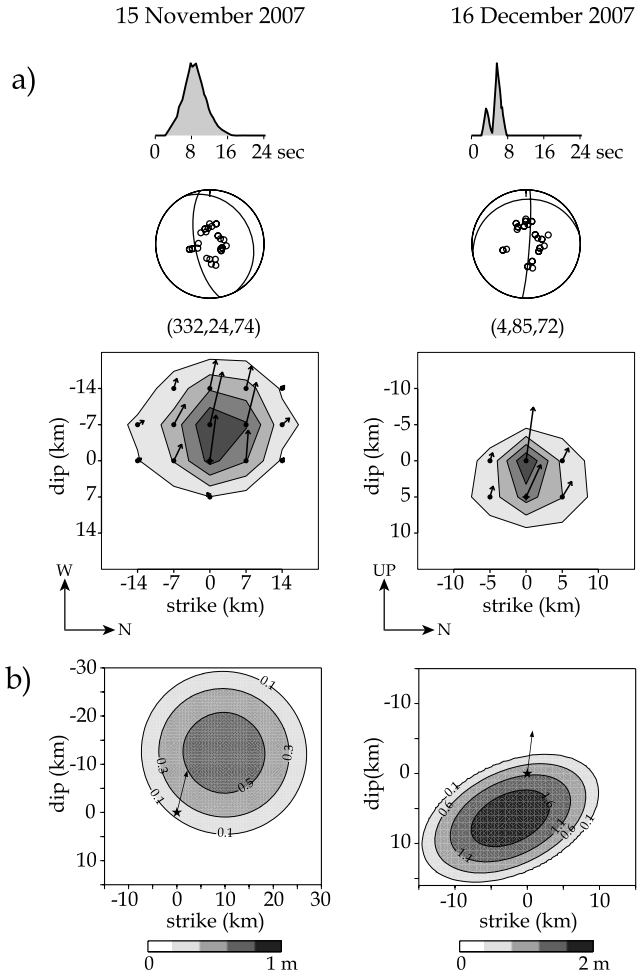

Figure 14. Near-field inversion of the main aftershocks of the Tocopilla earthquake of November 2007. Slip distributions for the 2007 November 15 and the 2007 December 16 events. (a) Teleseismic inversion: with, from top to bottom, source time functions, focal mechanisms and slip distributions and (b) slip distributions from strong-motion data inversion. Black arrows are the rake direction.

stresses accumulated since the 1877 mega-thrust earthquake were relieved in 2007 November. In contrast to the 1995 Antofagasta earthquake where, South of the Mejillones peninsula, most of the coupled zone ruptured; North of the peninsula, the shallower part of the coupled zone closest to the trench, does not seem to have ruptured in the 2007 November 14 event. It did rupture, however, at least partially, during some of the aftershocks of the main event.

The slip distribution determined for the 2007 Tocopilla earthquake is limited to the North by the rupture area of the $M_w = 7.4$, 1967 December 21 earthquake and to the South by the rupture zone of the 1995 July 30 Antofagasta earthquake. Ruegg *et al.* (1996), Chlieh *et al.* (2004) and Pritchard & Simons (2006) studied the coseismic and post-seismic slip produced by the Antofagasta earthquake. Coseismic slip initiated near the Mejillones Peninsula and the earthquake ruptured away from it toward the south with little coseismic slip below the peninsula. Pritchard & Simons (2006) also showed that the average rate of fault slip beneath the peninsula between 1995 and 2000 was nearly twice the plate convergence rate, concluding that the peninsula was not likely to rupture soon.

The slip distribution that we inverted from near- and far-field seismic data showed the presence of two distinct asperities. These asperities may represent stronger areas of the plate interface that had not slipped in the time lapse since the last major earthquake of 1877. Since the seismic activity of the Tocopilla area was very weak during the 20th century, slip in the areas between the asperities must have occurred aseismically. A more likely alternative scenario, in our opinion, is that the region between the two asperities of the Tocopilla earthquake had a stronger resistance to rupture because of the presence of a barrier. Such barriers have often been associated with some mechanical or geometrical features of the subducted plate. We can not decide from the present study whether an asperity or a barrier model is the more appropriate explanation for the presence of two distinct asperities in the Tocopilla earthquake. This is not really surprising, as shown by Thatcher (1990) and other authors, slip distributions of subduction zone earthquakes are often very complex with segments sometimes associated with subducted features of the ocean floor or with previous ruptures on the same plate interface (see, e.g. Robinson *et al.* 2006, for a recent discussion of this problem). For a sequence of earthquakes in the region of Ecuador-Colombia, Collot *et al.* (2004) propose a model of weak transverse faults which reduce coupling between adjacent

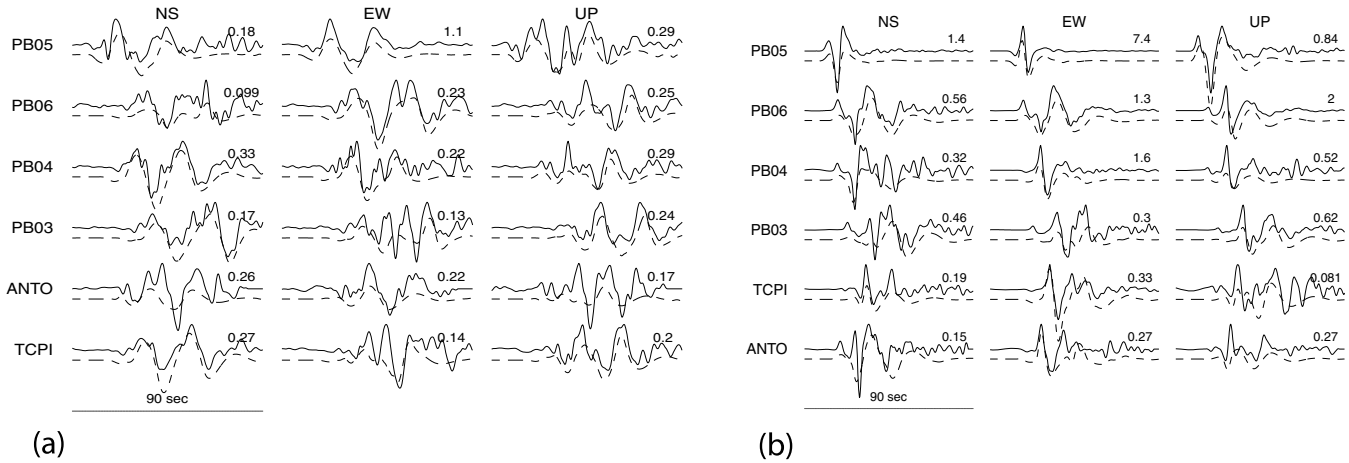

Figure 15. Near-field inversion of the main aftershocks of the Tocopilla earthquake of 2007 November. Strong-motion waveforms, accelerorgams were integrated into displacement and filtered between 0.04 and 0.25 Hz, observed records plotted with solid lines and synthetics with dashed lines, number right to each trace is the maximum value; (a) for 2007 November 15 event and (b) for the 2007 December 16 event.

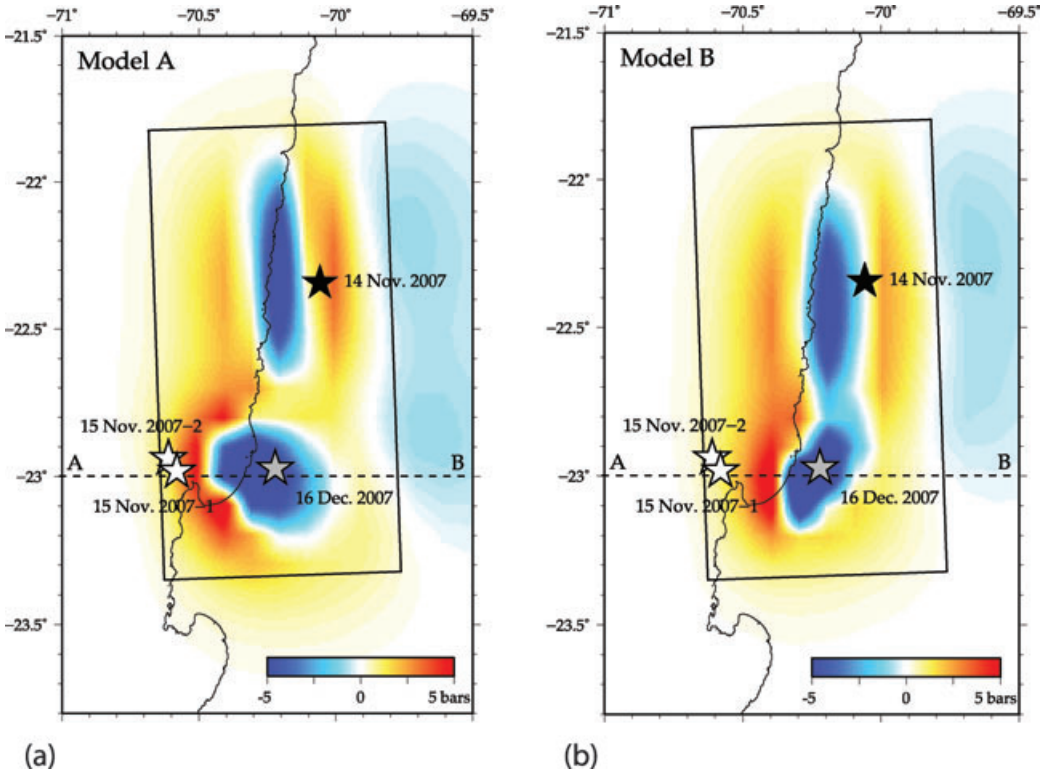

Figure 16. Stress transfer from the Tocopilla earthquake of 2007 November. Coulomb stress change associated with the mainshock (black star) at 30 km depth, based on the variable slip models A and B of the main event. Coulomb stress change was calculated on thrust faults with the mechanism of the two large aftershocks of 2007 November 15 (white stars). These two events occurred in region of stress increase (yellow to red regions). The 2007 December 16 event (grey star) is just shown here to locate it but it is not concern by the stress changes.

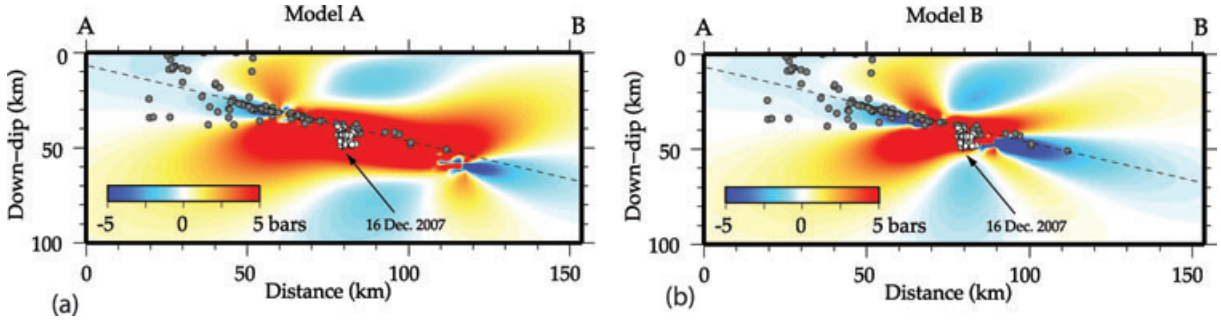

Figure 17. Cross-section of Coulomb stress change on a sub-vertical fault produced by the mainshock (cross-sections A–B is shown on the map on Fig. 16). Stress change is resolved on a fault with the same mechanism as the December 16 event. Aftershocks are plotted with grey to show the slab interface. The white dots show the aftershocks following the December 16 event. This slab-push event occurred in a region of stress increase.

segments. von Huene & Ranero (2002) imaged the deformation along the northern Chile margin with multibeam bathymetry, and revealed similar transverse fault zones that could correlate with the limits of the Tocopilla asperities.

In his study of Chilean earthquakes, Kelleher *et al.* (1973) divided the subduction zone into regions where great earthquakes of very long rupture lengths occur and regions where only moderate large earthquakes occur. A similar point of view was stated by Lay *et al.* (1982) who defined the typical Chilean-type subduction zones earthquakes as fault planes uniformly strong (all asperity) and rupture zone sizes are determined only by major transverse tectonic structures such as fracture zones and ridges. A simple interpretation of the seismic history of Northern Chile was that this region ruptured repeatedly with large subduction earthquake that broke the entire plate interface with fault length of several hundred km. Several explanations were given to this behaviour like the lack of sediments or the shallow dip of the seismogenic zone, or the shallow dipping seismogenic zone. The Tocopilla earthquake casts some doubt on this simple view of subduction zone seismicity.

The occurrence of the Tocopilla earthquake has important implications for the definition of seismic gaps. The subduction zone of Northern Chile was considered as a typical seismic gap where very large earthquakes like those of 1868 and 1877 may occur repeatedly with recurrence rates of a few hundred years. Closely connected with this assumption was the corollary that large earthquakes break the entire seismogenic zone from the trench to the transition zone. The Tocopilla of November 2007 is a clear counterexample to that

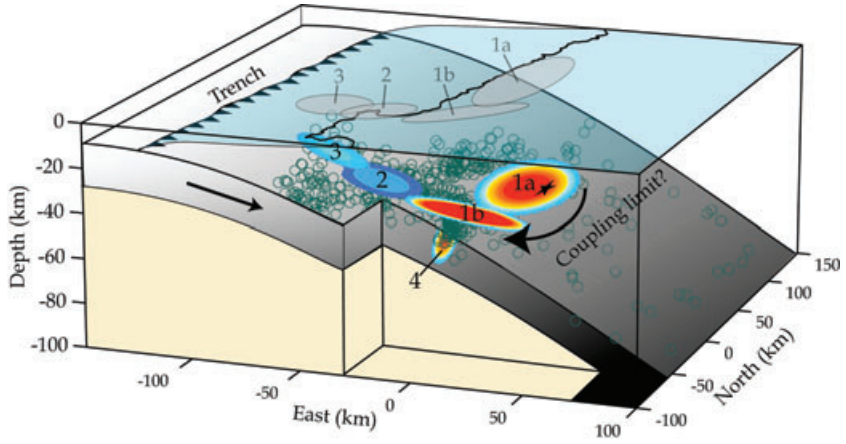

Figure 18. Summary of the rupture process of the $M_w = 7.6$ Tocopilla earthquake of 2007 November 14 and its main aftershocks. Slip distribution for the mainshock and its aftershocks: (1a and 1b) 2007/11/14 ($M_w = 7.6$); (2) 2007/11/15 at 15:03 ($M_w = 6.3$) and (3) 2007/11/15 15:06 ($M_w = 6.8$) is plotted along the plate interface. (4) The slab-push intraslab aftershock of 2007/12/16 intraslab ($M_w = 6.8$) cut through the plate interface. The grey ellipsoids are the slip projections at the surface. Greens circles are the preliminary aftershocks located by the Seismological service of Universidad de Chile.

simple classification of Chilean earthquake zones. This event broke only the deeper part of the seismogenic zone and was very similar in size and rupture extent to the repeated $M_w = 8$ earthquakes that have occurred in Central Chile near Valparaiso.

Although we cannot exclude that the Tocopilla event is a large foreshock of a future mega-thrust event, a more likely explanation in our opinion is that the seismogenic zones along the Chilean coast are the site of different-sized earthquakes, with very rare tsunamigenic events and more frequent events of magnitude close to 8. This scenario has some support from the seismicity of central Chile where a large tsunamigenic earthquake occurred in 1730 and then ruptured repeatedly with magnitude 8 events in 1821, 1906, 1971 and 1985 (Comte *et al.* 1986) and from the recent paleoseismic studies by (Vargas *et al.* 2005) in the Mejillones Peninsula who found two very large mega-thrust earthquakes, larger than that of 1877, and no trace of other events listed by (Comte & Pardo 1991) that were probably of magnitudes closer to 8.

Previous studies in the Andean subduction zones has found evidences that rupture length and coseismic slip vary between successive earthquake cycles in the same segment of the subduction zone (Kanamori & Mc Nally 1982; Collot *et al.* 2004). The rupture history suggested by the Tocopilla earthquake is actually very similar to that of the Ecuador-Colombia region where the inferred rupture area of the very large 1906 mega-thrust event ($M_w = 8.8$), was the site of by three thrust events in 1942 ($M_w = 7.8$), 1958 ($M_w = 7.7$) and 1979 ($M_w = 8.2$). The best known example of a segment of a subduction zone that sometimes rupture in a single great earthquake, but at other times breaks in a series of smaller events is that of the Nankai trough (Ando 1975). A simple interpretation of these variations is the asperity model proposed Kanamori & Mc Nally (1982) and Ruff (1992). A small earthquake represent failure of one asperity, and a great earthquake represent failure of several asperities depending on asperity interactions. Therefore the asperity model provides a self-consistent explanation for complex patterns of earthquake in subduction zones. And in the case of the Tocopilla earthquake, the asperity sizes have to be smaller than the interplate width, which could extend the concept of asperity model along subduction strike to asperity model along subduction dip.

Finally, several interesting questions remain that need to be carefully studied in the future. The main one is whether asperities defined from recent historical seismicity are persistent features or not. One crucial question is whether future earthquakes will break with a single rupture encompassing all of Northern Chile, or whether Northern Chile will enter a regime similar to that of Central Chile where earthquakes in the $M_w = 8$ magnitude range occur with shorter recurrence rates of the order of 80 years. Will large earthquakes migrate to the plate interface North of the 1967 earthquake or will they continue to rupture repeatedly the Southern portion again? The importance of long-term surveillance of seismic activity and the detection of possible slip transients in the area are of crucial importance for the full understanding of Northern Chile seismicity, to assess whether it is well organized in single periodic large earthquakes as is often assumed, or if it is as disorganized as seismicity elsewhere with regimes of smaller $M_w = 8$ events until tsunamigenic earthquakes like that of 1877 occur.

7 CONCLUSIONS

The Tocopilla earthquake of 14 November 2007 is the first large subduction earthquake in Chile that was well recorded by a set of near-field accelerometers. With this data and far field recordings we studied the rupture process of the earthquake. We obtained accurate fault plane solutions for the main shock and two aftershocks using waveform modelling. We successfully relocated the two subevents of the main shock and obtained a detailed view of the main features of slip distribution. The results of the inversions provide a picture of the rupture process of the main event that is consistent with a number of different data: earthquake locations, far and near-field seismic data as well as with the geodetic data inverted by Béjar-Pizarro *et al.* (2010).

The Tocopilla earthquake ruptured a 130 km long swath of the strongly coupled zone of plate interface between the Nazca and South American plates. In contrast to the 1995 Antofagasta earthquake, the Tocopilla earthquake did not break the entire plate interface relieving only partially the stress accumulated since the last major earthquake in the area, the 1877 Iquique mega-thrust earthquake. The remaining of the plate interface, oceanwards from the 2007 rupture zone may be still locked, or might have silently slipped during the main event or in the post-seismic period. Seismic data can not resolve this question, only geodetic observations currently being studied may shed some light on the very important question whether the stresses accumulated near Tocopilla were fully relaxed

during this event or whether this was only a foreshock to an even greater event that will rupture the entire plate interface. Continuous monitoring of the seismic and geodetic activity of the plate boundary may provide answers to this and other important questions about the rupture of long-standing seismic gaps.

ACKNOWLEDGMENTS

This research was carried out under the Montessus de Ballore International Laboratory established between the University of Chile and the Centre National de la Recherche Scientifique (CNRS) in France. The field operations were supported by grants from the Agence Nationale pour la Recherche (ANR-05-CATT-014, ANR-06-CATT-010-01). This work has been partially supported by the Nucleo Milenio IERC-MB project, Chile and the Spanish Ministerio de Educacion y Ciencia projects CGL2006-10311-C03-01and HP2007-089 and the Universidad Complutense (profesores UCM extranjero 2008). We thank C. Vigny for his help in establishing this project, and P. Bernard and P. Favreau for scientific discussions. Many researchers made possible this research, most notably A. Nercessian, S. Barrientos, M. Sobieziak, G. Meneses, A. Fuenzalida. We thank B. Schurr and other colleagues at GFZ who deployed the plate boundary stations in Northern Chile. We thank R. Boroschek of the Civil Engineering Department of Universidad de Chile for making their accelerometric data available for seismological research. We thank Sergio Ruiz for his careful reading of the manuscript. Finally, we thank the very useful and constructive comments by Dr Chen Ji and an anonymous reviewer.

REFERENCES

Ando, M., 1975. Source mechanisms and tectonic significance of historical earthquakes along the nankai trough, Japan, *Tectonophysics,* **27,** 119–140.

Angermann, D., Klotz, J. & Reigber, C., 1999. Space-geodetic estimation of the Nazca-South America Euler vector, *Earth planet. Sci. Lett.,* **171,** 329–334.

Araujo M. & Suárez, G., 1994. Geometry and state of stress of the subducted Nazca plate beneath central Chile and Argentina: evidence from teleseismic data, *Geophys. J. Int.,* **116,** 283–303.

Astiz, L. & Kanamori, H., 1986. Interplate coupling and temporal variations of mechanisms of intermediate-depth earthquakes in Chile, *Bull. seism. Soc. Am.,* **76,** 1614–1622.

Astroza, M. et al., 2008, Intensity and Damage Assessment of the 2007 Tocopilla Earthquake, Chile. Earthquake Engineering and Research Institute, Published online at http://www.eeri.org/site/content/view/156/35/.

Beck, S.L., Barrientos, S., Kausel, E. & Reyes, M., 1998. Source characteristics of historic earthquakes along the central Chile subduction zone, *J. S. Am. Earth Sci.,* **11,** 115–129.

Béjar-Pizarro, M., Carrizo, D., Socquet, A. & Armijo, R., 2010. Asperities and barriers on the seismogenic zone in North Chile: State of the art after the 2007 Mw 7.7 Tocopilla earthquake inferred by GPS and InSAR data. *Geophys. J. Int.*, submitted.

Boroschek, R., Comte, D., Soto, P. & Leon, R., 2008. Terremoto Norte Chile M=7.7, Informe preliminar. Published online at http://www.cec.uchile.cl/renadic/red.html.

Bouchon, M., 1981. A simple method to calculate Green's functions for elastic layered media, *Bull. seism. Soc. Am.,* **71,** 959–971.

Boore, D.M., 2001. Effect of baseline corrections on displacements and response spectra for several recordings of the 1999 Chi-Chi, Taiwan, earthquake, *Bull. seism. Soc. Am.,* **91,** 1199–1211.

Boore, D.M. & Bommer, J.J., 2005. Processing of strong-motion accelerograms: needs, options and consequences, *Soil Dyn. Earthq. Eng.,* **25,** 93–115.

Buske, S., Lüth, S., Meyer, H., Patzig, R., Reichert, C., Shapiro, S., Wigger, P. & Yoon, M., 2002. Broad depth range seismic imaging of the subducted Nazca Slab, North Chile, *Tectonophysics,* **350,** 273–282.

Casarotti, E. & Piersanti, A., 2003. Postseismic stress diffusion in Chile and South Peru, *Earth planet. Sci. Lett.,* **206,** 325–333.

Chlieh, M., de Chabalier, J.B., Ruegg, J.C., Armijo, R., Dmowska, R., Campos, J. & Feigl, K.L., 2004. Crustal deformation and fault slip during the seismic cycle in the North Chile subduction zone, from GPS and InSAR observations, *Geophys. J. Int.,* **158,** 695–711.

Cisternas, M. *et al.*, 2005. Predecessors of the giant 1960 Chile earthquake, *Nature,* **437,** 404–407.

Collot, J.Y. *et al.*, 2004. Are rupture zone limits of great subduction earthquakes controlled by upper plate structures? Evidence from multichannel seismic reflection data acquired across the northern Ecuador- southwest Colombia margin, *J. geophys. Res.,* **109,** B11103, doi:10.1029/2004JB003060.

Comte, D. & Pardo, M., 1991. Reapprisal of great historical earthquakes in the northern Chile and Southern Peru seismic gaps, *Nat. Hazards,* **4,** 23–44.

Comte, D., Eisenberg, A., Lorca, E., Pardo, M., Ponce, L., Saragoni, R., Singh, S.K. & Suárez, G., 1986. The central Chile earthquake of 3 March 1985: a repeat of previous great earthquakes in the region? *Science,* **233,** 449–453.

Coutant, O., 1990. Programme de Simulation Numérique AXITRA. Rapport LGIT, Université Joseph Fourier, Grenoble, France.

Delouis, B. & Legrand, D., 2007. Mw 7.8 Tarapacá intermediate depth earthquake of 13 June 2005 (northern Chile): Fault plane identification and slip distribution by waveform inversion, *Geophys. Res. Lett.*, **34,** doi:10.1029/2006GL028193.

Delouis, B. *et al.*, 1997. The $M_w = 8$ Antofagasta (Northern Chile) earthquake of 30 July 1995: a precursor to the end of the large 1977 gap, *Bull. seism. Soc. Am.,* **87,** 427–445.

Delouis, B., Pardo, M., Legrand, D. & Monfret, T., 2009. The Mw 7.7 Tocopilla Earthquake of 14 November 2007 at the Southern Edge of the Northern Chile Seismic Gap: rupture in the Deep Part of the Coupled Plate Interface, *Bull. seism. Soc. Am.,* **99,** 87–94.

Di Carli, S., Francois-Holden, C., Peyrat, S. & Madariaga, R., 2008. Kinematic and dynamic inversion of the 2000 Tottori earthquake based on elliptical subfault approximations, *Geophys. Res. Abstr.,* **11,** Abstract EGU2009-11330.

Engdahl, E.R. & Villaseñor, A., 2002. Global Seismicity: 1900 - 1999. In W.H.K. Lee, H., Kanamori, P.C. Jennings, and C. Kisslinger (editors), *International Handbook of Earthquake and Engineering Seismology*, Part A, Chapter 41, pp. 665–690, Academic Press, 2002.

Gardi, A., Lemoine, A., Madariaga, R. & Campos, J., 2006. Modeling of stress transfer in the Coquimbo region of central Chile, *J. geophys. Res.,* **111,** B04307, doi:10.1029/2004JB003440.

Giovanni, M.K., Beck, S.L. & Wagner, L., 2002. The June 23, 2001 Peru earthquake and the southern Peru subduction zone, *Geophys. Res. Lett.,* **29,** 2018, doi:10.1029/2002GL015774.

Graizer, V.M., 1979. Determination of the true ground displacement by using strong motion records. *Izvestiya, Earth Phys.,* **15,** 875–885.

Hartzell, S., Liu, P., Mendoza, C., Ji, C. & Larson, K.M., 2007. Stability and uncertainty of finite-fault slip inversions; application to the 2004 Parkfield, California, *Bull. seism. Soc. Am.,* **97,** 1911–1934.

Hébert, H., Boudin, F., Bernard, P., Peyrat, S. & Bejar, M., 2008. Tsunami modelling and source constraints from regional tide-gages and tilt measurements for the 2008 M=7.5, Tocopilla subduction earthquake, *EOS, Trans. Am. geophys. Un.,* **89,** Fall Meet. Suppl., Abstract OS43D-1338.

Husen, S., Kissling, E., Flueh, E. & Asch, G., 1999. Accurate hypocentre determination in the seismogenic zone of the subducting Nazca Plate in northern Chile using a combined on-/offshore network, *Geophys. J. Int.,* **138,** 687–701.

Iwan, W.D., Moser, M.A. & Peng, C.Y., 1985. Strong-motion earthquake measurement using a digital accelerograph, *Bull. seism. Soc. Am.,* **75,** 1225–1246.

Kanamori, H. & Mc Nally, K.C., 1982. Variable rupture mode of the subduction zone along the Ecuador-Colombia coast, *Bull. seism. Soc. Am.,* **72-4,** 1241–1253.

Kausel, E., 1986. Los terremotos de Agosto de 1868 y Mayo de 1877 que afectaron el Sur del Peru y Norte de Chile, *Boll. Acad. Chil. Ciencias,* **3,** 8–12.

Kausel, E. & Campos, J., 1992. The $M_s = 8$ tensional earthquake of 9 December 1950 of Northern Chile and its relation to the seismic potential of the region, *Phys. Earth planet. Int.,* **72,** 220–235.

Kelleher, J.A., 1972. Rupture Zones of Large South American Earthquakes and Some predictions, *J. geophys. Res.,* **77**(11), 2087–2103.

Kelleher, J., Sykes, L. & J. Oliver, J., 1973. Possible criteria for predicting earthquake locations and their application to major plate boundaries of the Pacific and the Caribbean, *J. geophys. Res.,* **78**(14), 2547–2585.

Kikuchi, M. & Kanamori, H., 1991. Inversion of complex body waves - III, *Bull. seism. Soc. Am.,* **81,** 2335–2350.

Klein, F.W., 1989. HYPOINVERSE, a program for VAX computers to solve for earthquake locations and magnitudes, *U.S. Geol. Survey Open-File Rep.*, 89–314, 59 pp.

Lancieri, M., Fuenzalida, A., Ruiz, S. & Madariaga, R., 2009. Magnitude Scaling of the early displacement for the 2007, Mw 7.8 Tocopilla sequence (Chile), *EOS, Trans. Am. geophys. Un.*, Jt. Assem. Suppl., Abstract S13A-1725.

Lay, T., Kanamori, H. & Ruff, L., 1982. The Asperity Model and the Nature of Large Subduction Zone Earthquakes, *Earthq. Predict. Res.,* **1,** 3–71.

Legrand, D., Delouis, B., Dorbath, L., David, C., Campos, J., Marquez, L., Thompson, J. & Comte, D., 2007, Source parameters of the Mw = 6.3 Aroma crustal earthquake of July 24, 2001 (Northern Chile), and its aftershock sequence, *J. South Am. Earth Sci.,* **24,** 58–68.

Lemoine, A., Madariaga, R. & Campos, J., 2002. Slab-pull and slab-push earthquakes in the Mexican, Chilean and Peruvian subduction zones, *Phys. Earth planet. Inter.,* **132,** 157–175.

Lin, J. & Stein, R.S., 2004. Stress triggering in thrust and subduction earthquakes, and stress interaction between the southern San Andreas and nearby thrust and strike-slip faults, *J. geophys. Res.,* **109,** B02303, doi:10.1029/2003JB002607.

Lomnitz, C., 1971. Grandes terremotos y tsunamis en Chile durante el periodo 1535-1955, *Geofis. Panamericana,* **1,** 151–178.

Lomnitz, C., 2004. Major Earthquakes of Chile: A Historical Survey, 1535-1960 Lomnitz. *Seism. Res. Lett.,* **75,** 368–378.

Madariaga, R., 1998. Sismicidad de Chile, *Física de la Tierra (Madrid),* **10,** 221–258.

Malgrange, M. & Madariaga, R., 1983. Complex distribution of large thrust and normal fault earthquakes in the Chilean subduction zone, *Geophys. J. R. astr. Soc.,* **73,** 489–505.

McCann, W.R., Nishenko, S.P., Sykes, L.R. & Krause, J., 1979. Seismic gaps and plate tectonics: seismic potential for major boundaries, *Pure appl. Geophys.,* **117,** 1082–1147.

McNally, K.C., 1983. Seismic gaps in space and time, *Ann. Rev. Earth Planet. Sci.,* **11,** 359–369.

Monelli, D. & Mai, P.M., 2008. Bayesian inference of kinematic earthquake rupture parameters through fitting of strong motion data, *Geophys. J. Int.,* **173,** 220–232.

Montessus de Ballore, F., 1911–1916. Historia Sismica de los Andes Meridionales, 6 vols. Cervantes, Santiago, Chile.

Nábělek, J., 1984. Determination of earthquake source parameters from inversion of body waves, *PhD thesis*, Massachusetts Institute of Technology, Cambridge, MA, USA.

Nishenko, S., 1985. Seismic potential for large and great interplate earthquakes along the Chilean and Southern Peruvian margins of South America: a quantitative reappraisal, *J. geophys. Res.,* **90,** 3589–3615.

Peyrat, S. & Favreau, P., 2010. Kinematic and spontaneous rupture models of the 2005 Tarapacá intermediate depth, *Geophys. J. Int.,* **181,** 369–381.

Peyrat, S. *et al.*, 2006. Tarapacá intermediate-depth earthquake (Mw 7.7 2005, northern Chile): a slab-pull event with horizontal fault plane constrained from seismologic and geodetic observations, *Geophys. Res. Lett.,* **33,** L22308, doi:10.1029/2006GL027710.

Pritchard, M.E. & Simons, M., 2006. An aseismic slip pulse in northern Chile and along-strike variations in seismogenic behavior, *J. geophys. Res.,* **111,** B08405, doi:10.1029/2006JB004258.

Pritchard, M.E., Ji, C. & Simons, M., 2006. Distribution of slip from 11 Mw > 6 earthquakes in the northern Chile subduction zone, *J. geophys. Res.,* **111,** B10302, doi:10.1029/2005JB004013.

Robinson, D.P., Das, S. & Watts, A.B., 2006. Earthquake rupture stalled by a subducting fracture zone, *Science,* **312,** 1203–1205.

Ruegg, J.C. *et al.*, 1996. The M W = 8.1 Antofagasta (North Chile) Earthquake of July 30, 1995: first results from Teleseismic and Geodetic Data, *Geophys. Res. Lett.,* **23**(9), 917–920.

Ruff, L.J., 1992. Asperity distributions and large earthquake occurrence in subduction zones, *Tectonophysics,* **211**(1-4), 61–83.

Ruiz, S., Lancieri, M., Madariaga, R., Sobiesiak, M. & Campos, J., 2009. Kinematic and dynamic inversion of the 16 December earthquake in Northern Chile, *EOS, Trans. Am. geophys. Un.*, Jt. Assem. Suppl., Abstract S34A-04.

Sambridge, M., 1999a. Geophysical inversion with a neigbourhood algorythm -I. Searching a parameter space, *Geophys. J. Int.,* **138,** 479–464.

Sambridge, M., 1999b. Geophysical inversion with neigbourhood algorythm -II. Appraising the ensemble, *Geophys. J. Int.,* **138,** 727–746.

Schurr, B. *et al.*, 2009. The International Plate Boundary Observatory Chile (IPOC) in the northern Chile seismic gap, *Geophysical Research Abstracts,* **11,** EGU General Assembly, EGU2009-11040.

Sobiesiak, M. *et al.*, 2008. The M 7.7 Tocopilla earthquake and its aftershock sequence: deployment of a Task Force local network, *EOS, Trans. Am. geophys. Un.,* **89,** Jt. Assem. Suppl., Abstract S24A-04.

Stauder, W., 1973. Mechanism of Spatial Distribution of Chilean Earthquakes with Relation to Subduction of the Oceanic Plate, *J. geophys. Res.,* **78,** 5033–5061.

Thatcher, W., 1990. Order and diversity in the modes of circum-Pacific earthquake recurrence, *J. geophys. Res.,* **95,** 2609–2623.

Tichelaar, B.W. & Ruff, L.R., 1991. Seismic coupling along the Chilean Subduction zone, *J. geophys. Res.,* **96,** 11 997–12 022.

Toda, S., Stein, R.S., Richards-Dinger, K. & Bozkurt, S., 2005. Forecasting the evolution of seismicity in southern California: anixmations built on earthquake stress transfer, *J. geophys. Res.,* **110,** B05S16, doi:10.1029/2004JB003415.

Vallée, M. & Bouchon, M., 2004. Imaging coseismic rupture in far field by slip patches, *Geophys. J. Int.* **156,** 615–630.

Vargas, G., Ortlieb, L., Chapron, E., Vald(c)s, J. & Marquardt, C., 2005. Paleoseismic inferences from a high resolution marine sedimentary record in northern Chile (23°S), *Tectonophysics,* **399,** 381–398.

von Huene, R. & Ranero, C.R., 2002. Subduction erosion and basal friction along the sediment-starved convergent margin off Antofagasta, Chile, *J. geophys. Res.,* **108,** 2079, doi:10.1029/2001JB001569.

SUPPORTING INFORMATION

Additional Supporting Information may be found in the online version of this article:

Supplement. To test the reliability of our models, we performed additional inversions. Figs S1 and S2 shows inversions similar to models A and B, but with variable rise time. For these models, during the inversion the rise time was variable and depended of the rupture velocity and spatial grid size. Rise time is defined to be the grid size divided by the rupture velocity. We also studied the effect of the frequency band chosen to filter the data on the kinematic inversion. Here we present an example for which we performed the inversion with displacement seismograms integrated from accelerograms and filtered in the 0.01–0.25 Hz frequency range. frequency band. We checked that 4 s is the highest resolution we can reach for our problem. We think that the station distribution does not allow us to resolve finer source features. The resolution is highly dependent on the number of stations, this seems to be the main limitation to resolving higher frequency features. The results are shown in

Figs S3 and S4. The models generated are very similar to models A and B obtained with data filtered in 0.01–01 Hz frequency ranges. They exhibit the same differences between them as models A and B.

Please note: Wiley-Blackwell is not responsible for the content or functionality of any supporting materials supplied by the authors. Any queries (other than missing material) should be directed to the corresponding author for the article.